Acta Neuropathologica Communications

RESEARCH

Open Access

Bridging the gap: investigating the role of phosphorylation at the serine 129 site of α-synuclein in VAPB-PTPIP51 interactions

Weijin Liu[1,2,3,4,5], Yongquan Lu[6,7], Jia Liu[8], Yan Yu[1,2,3,4,5*] and Hui Yang[9*]

Abstract

Parkinson's Disease (PD) is characterized by the aggregation and accumulation of α-synuclein (α-syn), along with abnormally high levels of α-syn phosphorylation at the serine 129 site (pSer 129 α-syn, p-α-syn). However, the mechanisms underlying the extensive phosphorylation at the serine 129 site in the pathogenesis of PD, as well as the role of p-α-syn in the process, remain unclear. Furthermore, though α-syn could bind to VAPB and loosen Endoplasmic Reticulum (ER)-mitochondria associations by disrupting VAPB-PTPIP51 tethers, whether and how the phosphorylation of α-syn at the serine 129 site regulates VAPB-PTPIP51 interactions, remains unclear. Herein, Co-Immunoprecipitation and Mass Spectrometry (CO-IP/MS) studies were preformed to identify and compare the Protein-Protein Interactions (PPIs) of phosphorylated and total α-syn in the midbrains of Thy1-SNCA transgenic mice. We further performed CO-IP and Molecular Dynamics (MD) simulation assays to confirm the influence of α-syn phosphorylation on the aforementioned interactions. Additionally, we performed Gene Ontology (GO) and Kyoto Encyclopedia of Genes and Genomes (KEGG) analyses to annotate the functional features of the common interacting proteins of p-α-syn and VAPB. The potential downstream proteins were further verified via CO-IP. According to the CO-IP and MD results, phosphorylation at the serine 129 site of α-syn increased VAPB-PTPIP51 interactions, and α-syn interacted directly with PTPIP51. Furthermore, functional and pathway enrichment analyses revealed that the common interacting proteins of p-α-syn and VAPB were significantly involved in protein binding, metal ion binding, structural constituent of the cytoskeleton, the intermediate filament cytoskeleton, and microtubule organization processes. Moreover, our findings confirmed the interactions of potential downstream target proteins (CLTC, CAMK2A, ATP1A3, and TUBB4B) with p-α-syn and VAPB. These findings collectively elucidate the structural underpinnings of serine 129 phosphorylation regulates the interaction between α-syn and both VAPB and PTPIP51. We hope that these findings will provide valuable insights into the role and regulatory mechanisms of serine 129 phosphorylation in the pathogenesis of pertinent diseases.

Keywords Parkinson's disease, α-synuclein, Serine phosphorylation, VAPB, PTPIP51

*Correspondence:
Yan Yu
yuyancrrc@163.com
Hui Yang
huiyang@ccmu.edu.cn

Full list of author information is available at the end of the article

Introduction

Parkinson's Disease (PD), a multisystem neurodegenerative disease with both motor and non-motor symptoms, has demonstrated an increasing prevalence with the aging global population [1, 2]. Notably, α-synuclein (α-syn), the primary component of proteinaceous inclusions in patients' affected tissues, has been associated with both familial and sporadic forms of PD [3, 4]. Furthermore, in-depth biomarker research on the detection of pathological α-syn (misfolded and aggregated) suggest that, α-syn pathology could serve as the gold standard for definitively diagnosing PD [3, 5]. Despite significant scholarly progress in elucidating α-syn pathology, its underlying pathophysiological mechanisms remain unclear [4]. Therefore, exploring the molecular mechanisms of α-syn pathology, a crucial therapeutic target, is imperative to halt or slow PD progression.

According to research, Posttranslational Modifications (PTMs) could influence the propensity of α-syn to misfold and aggregate [6]. Additionally, intensive studies targeting α-syn phosphorylation revealed unusually high α-syn phosphorylation levels at the serine 129 site of α-syn (pSer 129 α-syn, p-α-syn) in pathological α-syn inclusions, a modification crucially involved in α-syn aggregation, membrane association, internalization, and other processes [7–9]. As a result, various investigators have used p-α-syn antibodies to detect α-syn pathologies in multiple peripheral tissues and biofluids of PD patients during preclinical phases, highlighting the potential of p-α-syn as a diagnostic or progression biomarker for PD [6, 10–13]. For instance, through peptide pulldown assays and MS analyses, some researchers found that, unlike non-phosphorylated α-syn, the α-syn peptide phosphorylated at the serine 129 site was highly enriched in association with certain cytoskeletal proteins, vesicular trafficking proteins, and multiple enzymes [14]. Additionally, the GST-tagged recombinant Wild-type (Wt)/S129A mutant/S129D mutant h-α-syn (S129A and S129D mutations were employed to simulate the absence of phosphorylation and constitutive phosphorylation of serine 129 site, respectively.) was used as bait in previous research to enrich proteins in order to evaluate the interactions of phospho-incompetent and phospho-mimic h-α-syn in mouse brain [12]. Furthermore, a recent study employed biotinylation via antibody recognition to label total α-syn and p-α-syn in situ for subsequent MS analysis of brain tissues from patients [15, 16]. Despite these valuable research insights, the precise pathophysiological mechanisms of p-α-syn in PD pathologies, especially its roles relative to non-phosphorylated α-syn, remain unclear.

Increasing research evidence has associated PD pathologies with the dysfunction of Mitochondria-Associated Endoplasmic Reticulum (ER) Membranes (MAMs), signaling hubs involved in vital cellular processes such as calcium signaling, lipid metabolism, and autophagy [17, 18]. According to research, MAMs are enriched in specific proteins such as the membrane tether Vesicle-Associated Membrane Protein Associated Protein B (VAPB) and the outer mitochondrial membrane protein Tyrosine Phosphatase Interacting Protein 51 (PTPIP51) [19, 20]. Notably, VAPB is localized at the surface of the ER and acts as a receptor for protein partners [21]. Furthermore, it could interact with proteins relevant to PD. A *de novo* in-frame deletion of a valine residue at position 25 (p.ΔV25) in VAPB was detected in a sporadic PD case [22], highlighting the close association between VAPB dysfunction and PD pathogenesis. Moreover, α-syn was found in MAMs, and mutations in PD-related α-syn reduced its association with these MAMs [23, 24]. It is also noteworthy that previous Co-Immunoprecipitation (CO-IP) results showed that α-syn bound to the conserved N-terminal Major Sperm Protein (MSP) domain of VAPB but not to PTPIP51 [23]. Furthermore, although α-syn and PTPIP51 were found to bind to the MSP domain of VAPB [25, 26], these studies did not clearly define the VAPB-PTPIP51 interaction domains, and it remains unclear whether α-syn interacts directly with PTPIP51 [23].

To fully understand whether and how phosphorylation at the serine 129 site of α-syn regulates protein interactions, we first screened α-syn and p-α-syn antibodies with high affinity and specificity. We then used h-α-syn (Abcam, ab138501) and p-α-syn (CST, #23706) antibodies to capture total and phosphorylated α-syn in the midbrains of Thy1-SNCA transgenic mice. Subsequently, we identified and compared protein interactions via CO-IP and Mass Spectrometry (CO-IP/MS) studies. Biochemical techniques and Molecular Dynamics (MD) simulations were then employed to further confirm the influence of phosphorylation at the serine 129 site of α-syn and to predict the interaction domains in the α-syn-VAPB-PTPIP51, p-α-syn-VAPB-PTPIP51, α-syn-VAPB, and p-α-syn-VAPB complexes. Additionally, we performed Gene Ontology (GO) and Kyoto Encyclopedia of Genes and Genomes (KEGG) enrichment analyses to annotate the functional features of the common interacting proteins of p-α-syn and VAPB. Finally, we used CO-IP to validate the potential downstream proteins (CLTC, CAMK2A, ATP1A3, and TUBB4B) that interacted with p-α-syn and VAPB. Our findings, for the first time, to the best of our knowledge, revealed that phosphorylation at the serine 129 site of α-syn increased the interaction between VAPB and PTPIP51 and influenced the interacting proteins of VAPB. Notably, VAPB and PTPIP51 mainly interacted with the C-terminus of α-syn (90-140AA) and the N-terminus of α-syn (1-60AA), respectively. Furthermore, in pathological circumstances,

p-α-syn and VAPB correlated closely with protein binding, metal ion binding, structural constituent of the cytoskeleton, the intermediate filament cytoskeleton, and microtubule organization pathways. Overall, in addition to elucidating the structural basis of how serine 129 phosphorylation regulates the Protein-Protein Interaction (PPIs) of α-syn and downstream pathways, our findings also reveal a novel regulatory mechanism of serine 129 phosphorylation in α-syn pathology.

Materials and methods

Animals

Herein, human α-syn (h-α-syn) overexpressing transgenic mice [JAX stock #017682; C57BL/6 N-Tg (Thy1-SNCA) 15Mjff/J; hemizygotes] and Wild-type (Wt) C57BL mice (both from Jackson Laboratory, Bar Harbor, ME, USA), as well as α-syn Knock-Out (KO) mice (C57BL/129 × 1-Sncatm1Rosl/J; Model Animal Research Center of Nanjing University) were used. All animals were on the BALB/6 background and were housed at Room Temperature (RT) conditions under a 12 h: 12 h light/dark cycle in SPF animal facility of China Rehabilitation Research Center [SYXK (Beijing) 2015-0047]. All animal experiments adhered to the National Institute of Health's (NIH; Bethesda, MD, USA) animal care and use guidelines. Capital Medical University's Institutional Animal Care and Use Committee (Capital Medical University Animal Experiments and Experimental Animals Management Committee, AEEI-2023-247 and AEEI-2022-073) reviewed and approved the study protocol.

Western Blotting (WB)

We performed WB as outlined in previous research [27, 28]. Briefly, samples of recombinant protein (h-α-syn/p-α-syn, 200 ng/lane), cell lysate, and mice midbrain homogenate (mixed with 1 X protease inhibitors and phosphatase inhibitors cocktail; all from ServiceBio) were first mixed with loading buffer (250 mM Tris-HCl, pH 6.8, 30% glycerol, and 0.02% Bromophenol Blue) and then incubated at 95°C for 10 min. After denaturation, protein samples were separated using 10% and 12% Sodium Dodecyl Sulfate Polyacrylamide Gel Electrophoresis. The gels were then transferred to Polyvinylidene Difluoride (PVDF) membranes (0.22 μm, ISEQ00010, Millipore) at 2 mA/cm^2 for 90 min. For α-syn and p-α-syn detection, the membranes were incubated with 0.4% paraformaldehyde (PFA) for 30 min and then washed three times with TBST. After being blocked with 5% skimmed milk for 1 h at RT, the membranes were incubated with primary antibodies against h-α-syn (ab138501, Abcam, 1/2,000), p-α-syn (#23706, CST, 1/2,000), α-syn (Sc69977, Santa Cruze, 1/1,000), VAPB (14477-1-AP, Proteintech, 1/1,000), PTPIP51 (20641-1-AP, Proteintech, 1/1,000), CLTC (26523-2-AP, Proteintech, 1/2,000), CAMK2A (13730-1-AP, Proteintech, 1/1,000), ATP1A3 (10868-1-AP, Proteintech, 1/500), Beta-Tubulin (10094-1-AP, Proteintech, 1/2,000), and β-actin (AC026, ABclonal, 1/4,000) at 4 °C. The membranes were then washed three times with TBST and incubated with secondary antibodies at RT for 1 h with gentle agitation to facilitate comprehensive binding to the primary antibodies. For WB following immunoprecipitation (IP), a conformation-specific anti-rabbit IgG secondary antibody for IP, conjugated with horseradish peroxidase (HRP) (RA1008-01, Vazyme, 1/2,000), was employed to detect CAMK2A (50 kDa) and TUBB4B (55 kDa). This method ensured that the detection was not confounded by the denatured light chain (25 kDa) or heavy chain (55 kDa) of the IP antibody. Following that, the membranes were washed three times with TBST and enhanced chemiluminescence chromogenic substrate (E422-01, Vazyme) was employed for protein visualization, and the chemical fluorescence from blots was photographed and scanned using a ChemiDoc MP imaging system (Bio-Rad). In other experimental conditions, fluorophore-conjugated secondary antibodies, including mouse 680 (926-68070; LI-COR Biosciences, Lincoln, NE, USA) and rabbit 680 (926-68071; LI-COR Biosciences, USA), diluted 1/10,000, were utilized. The fluorescence from blots were visualized in an Odyssey imaging system (LI-COR Biosciences, USA).

Co-immunoprecipitation (CO-IP) assay

CO-IP method is similar to that previously reported [29]. First, protein concentrations in brain homogenates and cell lysates were determined using the Bicinchoninic Acid BCA assay kit (23225, Thermo Scientific). Subsequently, 2,000 μg brain homogenates or 1,500 μg cell lysates were incubated with IP antibodies or rabbit IgG (2729S, CST) in a 400 μL IP buffer system (25 mM Tris-HCl, 150 mM NaCl, 1 mM EDTA-Na_2, 1% NP-40, 1 X protease inhibitors, and phosphatase inhibitors cocktail; all from ServiceBio). The IP antibodies included h-α-syn (ab138501, Abcam, 1/200), p-α-syn (#23706, CST, 1/50), VAPB (14477-1-AP, Proteintech, 1/60), CLTC (26523-2-AP, Proteintech, 1/60), and Flag (C1305, Applygen, 1/100). The mixture was incubated with constant rotation for 16 h at 4 °C. Following that, 30 μL Protein A/G Magnetic Beads (HY-K0202, MCE) were added into the system and incubated for 6 h at 4 °C. The bead–antigen-antibody complex was separated using a magnetic rack. The supernatant (40 μL, Output fraction) was mixed with 10 μL 5 X loading buffer, and the bead–antigen-antibody complex (IP fraction) was mixed with 30 μL 2 X loading buffer. Both mixtures were then incubated at 95°C for 10 min.

Cell culture and transfection

First, SHSY5Y human neuroblastoma cells (The Cell Bank of the Chinese Academy of Science, BFN60700126, Shanghai, China) were cultured in a DMEM-F12 medium (11320033, Gibco) supplemented with 10% Fetal Bovine Serum (FBS) and 1% penicillin/streptomycin. Plasmids Flag-PTPIP51 (NM_018145, Vigene) and myc/myc-h-α-syn/myc-S129A (CH884935, Vigene) were then transiently co-transfected into SHSY5Y cells using Transporter 5 Transfection Reagent (26008–1A, Polysciences). After 48 h of transient transfection, the cells were harvested and cell lysates were extracted via treatment with an IP buffer (25 mM Tris-HCl, 150 mM NaCl, 1 mM EDTA-Na_2, 1% NP-40, 1 X protease inhibitors and phosphatase inhibitors cocktail; all from ServiceBio). Finally, the lysates were sonicated and centrifuged at 12,000 x g for 30 min at 4 °C, before collecting the supernatant and storing, awaiting IP tests.

Molecular docking

The complete 3D structure of PTPIP51 was predicted using AlphaFold 2 [30]. The complex structure between VAPB dimer with α-syn/p-α-syn, PTPIP51 with α-syn/p-α-syn were predicted using AlphaFold3 [31]. The molecular visualizations were carried out using PyMOL software (Version 1.8. 2015). On the other hand, the complex interaction of VAPB dimer with PTPIP51, and of α-syn with VAPB-PTPIP51, were predicted using HDOCK [32]. The grid spacing was set to 1.2 Å for a 3D translational search and the angle interval was set to 15 degrees for rotational sampling in the 3D Euler space. All docked poses were ranked based on scoring to generate 100 poses, with the highest ranked pose selected as the final binding mode.

Molecular dynamics (MD) simulation

Herein, MD simulation was performed with GROMACS (version 2020.6) for the complexes of α-syn-VAPB-PTPIP51, p-α-syn-VAPB-PTPIP51, α-syn-VAPB, and p-α-syn-VAPB. The AMBER14 Force Field and General AMBER Force Field (GAFF) parameters were employed for the protein and mutant residue Serine 129 (defined as SEP129) of α-syn, respectively. The partial atomic charges of SEP129 were determined using the Restrained Electrostatic Potential (RESP) charge following the optimization of SEP129 at the B3LYP/6-31G (d) level with the Gaussian16 package. Subsequently, sodium counter ions were added to neutralize the complexes, which were solvated in a box with TIP3P water molecules. The solvent layers between the box edges and the solute surface were set to 1.2 nm.

The long-range electrostatic interactions were treated with the Particle Mesh Ewald (PME) method and the cutoff for van der Waals interactions was set to 1.0 nm. Before the production run, the systems were relaxed for 1,000 steps using the steepest descent algorithm, followed by an additional 1,000 steps using the conjugate gradient method. The temperature and pressure in the equilibration phase were controlled using the Berendsen coupling algorithm, with time constants of 0.1 and 1.0 ps, respectively. Furthermore, the protein was constrained to allow for the relaxation of water molecules over 100 ps. For the production run, an integration time step of 2 fs was employed to integrate the motion equations. The simulation systems' temperatures were controlled and kept constant using the V-rescale thermostat algorithm. On the other hand, the Parrinello-Rahman coupling algorithm was used to keep the pressure constant. The simulated temperature and pressure were set to 298.15 K and 1 bar, respectively. The MD simulation was performed in the NPT ensemble within 200 ns. The binding free energy of proteins between each chain was determined using gmx_MMPBSA (Version 1.4.3) with MMPBSA.py from the AmberTools20 suit. Molecular visualizations were preformed using PyMOL software.

Preparation of h-α-syn and p-α-syn proteins

First, the purified recombinant protein was extracted from the bacterial lysate by combining it with glutathione Sepharose 4B (17-0756-01, GE Health) as outlined in previous research [33]. After induction with 0.1 mM Isopropyl-β-D-1-Thiogalactopyranoside (IPTG) for 2.5 h, GST-human-α-syn/mouse-α-syn (h-α-syn/m-α-syn) was expressed, and α-syn was collected after digestion with human thrombin for 6 h at RT. The elution buffer for α-syn was changed into a working buffer (20 μM HEPES, 10 μM $MgCl_2$, 20 μM dithiothreitol, pH 7.4) using a 10 kD molecular weight cut off filter. Polo-Like-Kinase 3 (PLK3) was used to produce the p-α-syn monomer. The reaction system comprised 50 μL α-syn (2 mg/mL), 1.2 μL PLK3 (PV3812, ThermoFisher Scientific), and 0.5 μL ATP (A26209-1G, Sigma). After incubation for 3 h in a 30 °C water bath, the reaction was terminated using 25 mM EDTA-Na_2. The resultant α-syn and p-α-syn were then verified with antibodies via WB.

In-gel solution digestion

Shanghai Genechem Co., Ltd performed the LC-MS/MS analysis as outlined in previous research [34]. Briefly, purified protein samples prepared in the CO-IP stage were separated using SDS-PAGE. The desired pieces were then excised and split evenly into about 1 mm^3 sizes for every gel slice. Subsequently, 1 mL destaining buffer (100 mM NH_4HCO_3/30% ACN) was added for destaining until a transparent solution was realized. The gel slices were dried after discarding the supernatant. The proteins were reduced with 10 mM DTT (in 100 mM NH_4HCO_3) for 30 min at 56 °C, after which the supernatant was

discarded. Subsequently, the ACN was added and incubated for 5 min before discarding the supernatant. Following that, 60 mM Iodoacetamide (IAA) was added to block the cysteine residues and incubated for 20 min in the dark, after which the supernatant was discarded. Subsequently, 200 mM NH_4HCO_3 was added and incubated for 15 min at RT before discarding the supernatant. The ACN was then added again and incubated for 5 min before discarding the supernatant and drying the gel slices. Following that, 200 ng (20 ng/μL) trypsin was added and incubated for 30 min at 4 °C after which 40 μL 25 mM NH_4HCO_3 was added and incubated overnight at 37 °C. The supernatant was then collected and transferred to another new tube. After adding 60% ACN/0.1% TFA in the first tube, the solutions were combined and transferred to a new tube after ultrasonication for 15 min. Following that, the pooled solution was lyophilized. The whole peptide sample was re-suspended in 0.1% TFA, desalted with the C18 Cartridge, and then re-suspended in 10 μL 0.1% formic acid.

LC-MS/MS assays and data analysis

The LC-MS/MS analysis was performed using a Q Exactive mass spectrometer coupled with an Easy nLC (ThermoFisher Scientific). First, the peptide sample was loaded onto the C18-reversed phase analytical column (ThermoFisher Scientific, Acclaim PepMap RSLC 50 μm X 15 cm, nano viper, P/N164943) in buffer A (0.1% formic acid in HPLC grade water), and then separated with a linear gradient of buffer B (80% acetonitrile and 0.1% Formic acid) at a flow rate at 300 nL/min. Subsequently, the peptide was entered into the Q Exactive mass spectrometer. The raw data obtained was imported into Proteome Discoverer 2.2 for protein identification, after which, database searches were performed using embedded Mascot 2.6 engines. A precursor mass tolerance of 10 ppm was specified, and a 0.05 Da tolerance was set for MS2 fragments ions. Protein identification was considered positive if the peptide score of a specific peptide exceeded the significance threshold (FDR = 0.01).

Enrichment analysis

The GO and KEGG functional enrichment analyses on p-α-syn and VAPB interacting proteins in the midbrain of Thy1-SNCA transgenic mice were perform using the DAVID database (https://david-d.ncifcrf.gov/). The top 10 GO and KEGG terms of p-α-syn and VAPB common interactome proteins were then listed. Venn diagrams were plotted using an online platform for data analysis and visualization (https://www.bioinformatics.com.cn; last accessed on 20 June 2024).

Statistical analysis

Statistical analyses were performed using Prism 8.0.1 software (GraphPad, La Jolla, CA, USA). Each experiment was independently conducted at least three times, and the results are presented as the mean ± standard error of the mean (SEM). Differences in the p-α-syn/h-α-syn ratio in SHSY5Y cells or α-syn/p-α-syn levels in mouse brain tissues were assessed using the unpaired t-test. Other datasets were analyzed using one-way ANOVA followed by Tukey's multiple comparisons test. In all cases, a value of $P < 0.05$ was considered statistically significant.

Results

Identification of h-α-syn and p-α-syn interacting proteins via LC-MS/MS analysis of CO-IP products in midbrain of Thy1-SNCA transgenic mice

Previous research has indicated that duplications and triplications of the *SNCA* gene, which encodes α-syn, are responsible for autosomal dominant familial PD [35]. Additionally, it has been reported that the levels of α-syn can significantly influence the disease phenotype. The severity of the familial Parkinsonian phenotype is contingent upon the dosage of the *SNCA* gene and the corresponding protein levels [36]. Herein, we used a transgenic (Tg) mouse model (Thy1-SNCA Tg mice), that overexpressed human α-syn (h-α-syn) under the control of the mouse Thy1 promoter. This transgenic line could mimic familial forms of PD, exhibiting typical progression of nonmotor and motor symptoms that are exacerbated with age [11, 28, 37]. Western Blotting (WB) analysis revealed that the midbrain of Tg mice exhibited significantly elevated levels of α-syn compared to Wt mice, with an increase of approximately 2–3 fold, as illustrated in Supplementary Material. Figure 3 A, I. This observation aligns with our prior findings, which demonstrated an upregulation of h-α-syn and p-α-syn in the midbrain of 13-month-old Tg mice [33]. To further identify proteins involved in α-syn pathology, this study sought to detect proteins interacting with h-α-syn and p-α-syn in the midbrain of Tg mice. Specifically, we performed CO-IP assays with h-α-syn (Abcam, ab138501) and p-α-syn (CST, #23706) antibodies, and then subjected the bands of interest to MS analysis (Fig. 1A). Protein complexes were further pulled down and detected via WB using the above-indicated antibodies. According to the results, h-α-syn and p-α-syn exhibited significantly enrichment when bound to antibodies, compared to non-immune IgG. Meanwhile, the midbrain of α-syn Knock-Out (KO) mice barely exhibited any enrichment (Fig. 1B-C). Subsequently, we subjected the IP protein complexes to electrophoresis and confirmed them via in-gel digestion and proteomics analyses. Our CO-IP/MS identified 205 and 225 proteins (Peptides 95% ≥ 2) as putative binding

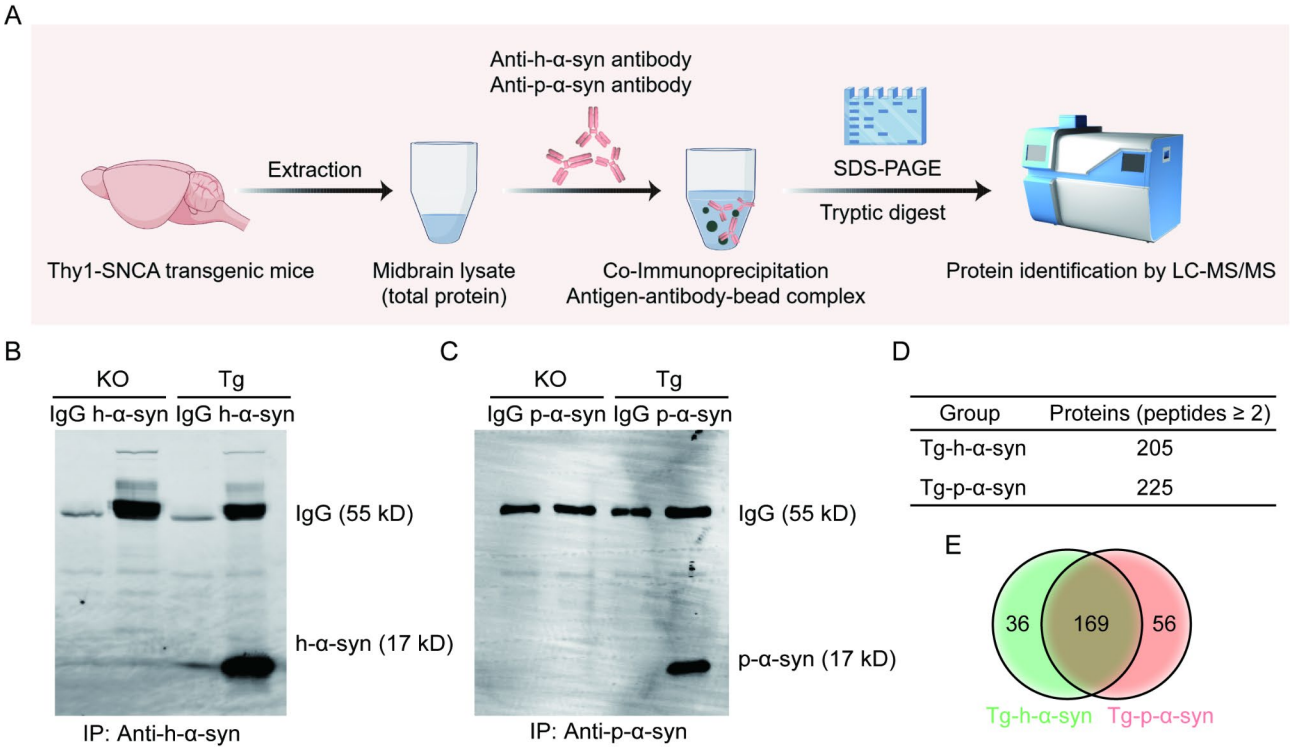

Fig. 1 LC-MS/MS identification of h-α-syn and p-α-syn interacting proteins in the midbrain of Thy1-SNCA transgenic mice **A.** Flowchart showing the experimental procedures used for identification of h-α-syn and p-α-syn interacting proteins in the midbrain homogenates of Thy1-SNCA transgenic (Tg) by mass spectrometry. By Figdraw. **B-C**. WB of proteins immunoprecipitated from the midbrain of Tg mice, extracted by h-α-syn antibody (**B**) and p-α-syn antibody (**C**). **D**. Proteins identified with a minimum of 2 unique peptides (Peptides 95% ≥ 2) were included in analyses (Supplementary Material. Table 7). **E**. Venn diagrams displaying the degree of overlap in numbers of proteins, which differentially interacted with h-α-syn and p-α-syn. The green area displays proteins interacting specifically with h-α-syn (includes 36 proteins), the pink area displays proteins interacting specifically with p-α-syn (includes 56 proteins), the brown area displays proteins interacting with both h-α-syn and p-α-syn (includes 169 proteins). h-α-syn was analyzed with h-α-syn antibody (Abcam, ab138501), p-α-syn was analyzed with p-α-syn antibody (CST, #23706). The midbrain homogenates derived from the 13 months-old α-syn knockout (KO) mice and Tg mice were used, normal rabbit IgG served as the negative control. IP, immunoprecipitation

partners of h-α-syn and p-α-syn, respectively (Fig. 1D, Supplementary Material. Table 8, and 9). Interestingly, the h-α-syn and p-α-syn interacting proteins exhibited an unexpected divergence, implying that, as one of the most common PTM, phosphorylation of α-syn at the serine 129 site could be crucial in modulating its interactions with relevant proteins (Fig. 1E, Supplementary Material. Table 7).

Phosphorylation at the serine 129 site of α-syn increased the interaction between VAPB and PTPIP51

LC-MS/MS results for the Tg midbrains showed that p-α-syn could interact with VAPB and PTPIP51. PTPIP51 ranked first and VAPB ranked sixth in all the differential interacted proteins (specifically interacted with p-α-syn but not h-α-syn) (Fig. 2A, Supplementary Material. Table 7). Therefore, among the 56 proteins potentially interacting with p-α-syn, our study concentrated on PTPIP51 and VAPB. It is well established that VAPB, the integral Endoplasmic reticulum (ER) protein, binds to PTPIP51, the outer mitochondrial membrane protein, forming a set of tethers that, regulate multiple key cellular processes [17, 25, 38, 39]. Although α-syn was found to bind to VAPB and the overexpression of Wild-type and familial PD's disease mutant α-syn (A53T mutant/A30P mutant) was reported to loosen ER-mitochondria associations by disrupting VAPB-PTPIP51 tethers [23], whether and how phosphorylation of α-syn at the serine 129 site regulates interactions between VAPB and PTPIP51 remain unclear. For insights into the underlying mechanisms of the phosphorylation of α-syn at the serine 129 site impacts VAPB-PTPIP51 interaction, we first established whether p-α-syn bound to VAPB and PTPIP51. The binding of h-α-syn/p-α-syn to PTPIP51 and VAPB was monitored using IP assays involving SHSY5Y cells co-transfected with Flag-PTPIP51 and myc-h-α-syn. Our findings confirmed the interaction between p-α-syn and the VAPB-PTPIP51 complex. Moreover, for the first time, to the best of our knowledge, we found that phosphorylation of α-syn at the serine 129 site increased its interaction with the VAPB-PTPIP51 complex (Fig. 2B-C). Building on this foundation, we conducted a further investigation into whether phosphorylation of α-syn at the serine 129 site regulates the interaction between

A

Accession	Name	Peptides (95%)	%Cov
sp|Q3UJU9|	PN: Regulator of microtubule dynamics protein 3 (Rmdn3), or Protein tyrosine phosphatase interacting protein 51 (PTPIP51); GN=Rmdn3; PE=1; SV=2;	10	33.190000
sp/tr|Q8BH80|	PN: Vesicle-associated membrane protein, associated protein B and C; GN=Vapb; PE=1; SV=1;	5	30.860001

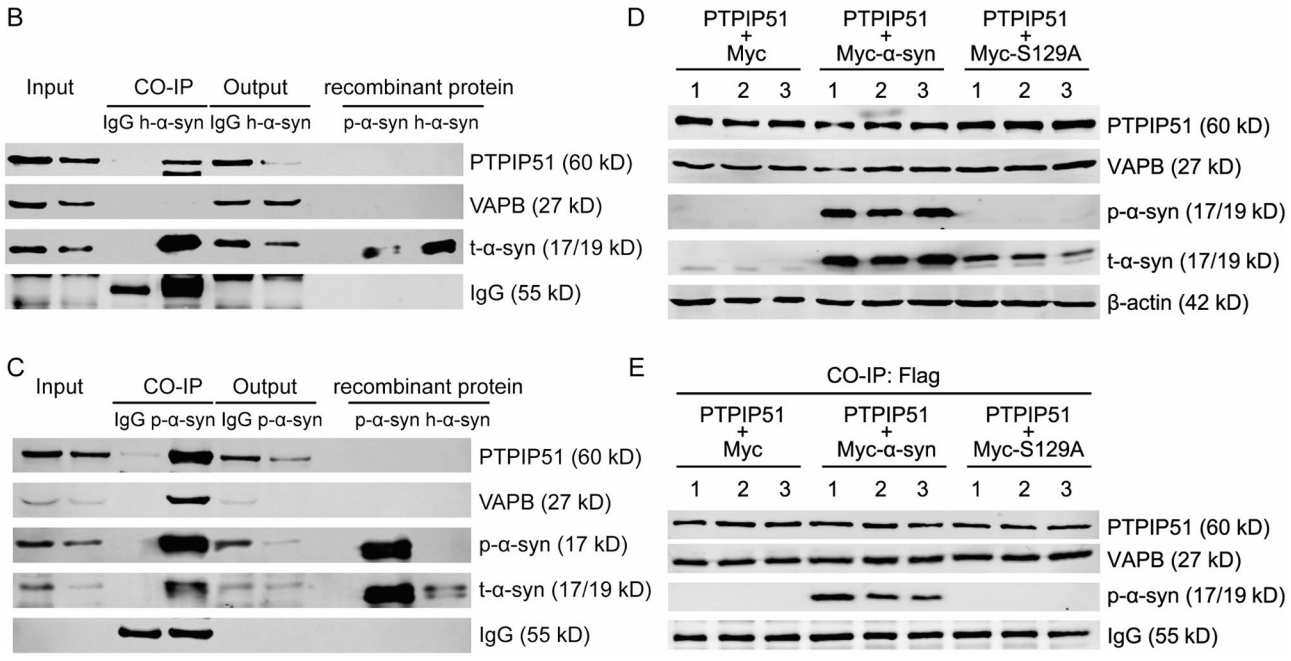

Fig. 2 Post-transcriptional phosphorylation modification at the serine 129 site of α-syn can promote the interaction between α-syn and VAPB-PTPIP51 complex **A**. LC-MS/MS results for the Tg midbrains showed that p-α-syn could interact with VAPB and PTPIP51. PTPIP51 ranked first and VAPB ranked sixth in all the differential interacted proteins (specifically interacted with p-α-syn but not h-α-syn). Flag-PTPIP51 and myc/myc-h-α-syn/myc-S129A expression plasmids were transiently co-transfected into SHSY5Y cells. After 48 h, the cell lysates were extracted and subjected to WB and CO-IP. **B-C**. CO-IP and WB analyses of the interaction between h-α-syn/p-α-syn and VAPB/PTPIP51. The cell lysates were subjected to the IP assay using the anti-h-α-syn antibody (**B**) and anti-p-α-syn antibody (**C**) followed by WB with the indicated antibodies. **D**. WB analysis of the protein expression of PTPIP51, VAPB, p-α-syn, and t-α-syn. **E**. CO-IP and WB analyses of the interaction between VAPB and PTPIP51. The cell lysates were subjected to the IP assay using the anti-flag antibody followed by WB with VAPB and PTPIP51 antibodies. 200 ng recombinant p-α-syn and h-α-syn proteins were used as positive controls in CO-IP experiments. t-α-syn, total α-syn

VAPB-PTPIP51. It has been reported that the Wt/A53T mutant/A30P mutant α-syn does not alter the expression levels of VAPB or PTPIP51 [23]. In this study, SHSY5Y cells were transiently co-transfected with Flag-PTPIP51 and myc/myc-h-α-syn/myc-S129A mutant α-syn (S129A) expression plasmids. After 48 h, cell lysates were collected and analyzed via WB. Our WB results found that the overexpression of α-syn and S129A did not affect the expression of VAPB or PTPIP51 (Fig. 2D, Supplementary Material. Figure 2A, D, E). Subsequently, the cell lysates underwent CO-IP using an anti-Flag antibody, followed by WB analysis with VAPB and PTPIP51 antibodies. The results indicated that neither α-syn nor S129A reduced the amount of endogenous VAPB bound to Flag-PTPIP51 (Fig. 2E, Supplementary Material. Figure 2B, F).

Phosphorylation at the serine 129 site of α-syn influenced the dynamics of the α-syn-VAPB-PTPIP51 complex

As a member of the VAPs family, VAPB contains a highly conserved N-terminal major sperm protein (MSP, 1-125AA) domain, which interacts with a short, conserved peptide motif named FFAT (two phenylalanines in an acidic tract) in various of membrane-associated proteins [21, 40]. Although both of α-syn and PTPIP51 could bind to the MSP domain of VAPB, the regions of α-syn and PTPIP51 mediating these interactions remain unclear [23, 25, 26]. Therefore, we performed Molecular dynamics (MD) simulation to explore the interaction mechanisms using GROMACS (version 2020.6). First, a 3D structure of human PTPIP51 was predicted using AlphaFold 2 [30]. Following that, the complex dimeric crystal structure of the Wild-type human VAPB MSP

domain (PDB entry 3IKK) with both PTPIP51 and α-syn (PDB entry 1XQ8), as well as the VAPB-PTPIP51 complex, was predicted using HDOCK [32]. All docked poses were ranked based on scoring to generate 100 poses, with the highest ranked pose selected as the final binding mode.

According to the results, the Root Mean Square Deviation (RMSD) of the α-syn-VAPB-PTPIP51 complex tended to be in a horizontal line, indicating that this system achieved an equilibrium state within the simulation time (Fig. 3A, blue line). On the other hand, the analysis of Root Mean Square Fluctuation (RMSF) suggested that the protein fluctuated within a reasonable range (Supplementary Material. Figure 4 A-E, blue line). Figure 4 A shows the simulation outcome with the most energetically favorable binding pose of the α-syn-VAPB-PTPIP51 complex. Tables 1 and 2 show the contact lists for VAPB with PTPIP51, α-syn with VAPB, and α-syn with PTPIP51 in the α-syn-VAPB-PTPIP51 complex.

We further performed MD simulations to detect the binding patterns of the mutant α-syn-VAPB-PTPIP51 complex (p-α-syn-VAPB-PTPIP51) in order to establish the influence of the phosphorylation of α-syn at the serine 129 site on the stability of the VAPB-PTPIP51 tether. According to the RMSD results, the p-α-syn-VAPB-PTPIP51 system achieved an equilibrium state within the simulation time (Fig. 3A, red line). On the other hand, the RMSF analysis suggested that the protein fluctuated within a reasonable range (Supplementary Material. Figure 4 A-E, red line). Figure 4B shows the binding mode for the p-α-syn-VAPB-PTPIP51 complex. Tables 3 and 4 show the contact lists for VAPB with PTPIP51, p-α-syn with VAPB, and p-α-syn with PTPIP51 in the p-α-syn-VAPB-PTPIP51 complex.

A

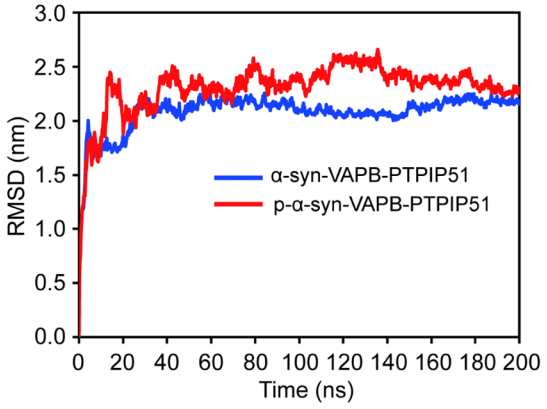

D

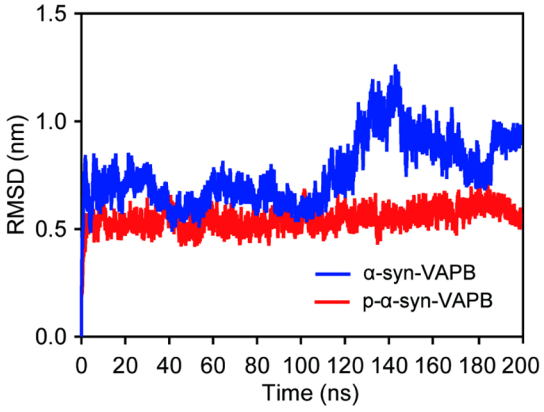

B

Contribution	VAPB-PTPIP51	α-syn-VAPB	α-syn-PTPIP51
ΔEvdw	-173.96	-63.61	-106.57
ΔEele	-462.04	-1226.79	595.02
ΔGpolar	566.74	1264.00	-548.37
ΔGnonpolar	-27.72	-10.90	-14.85
ΔGtotal	-96.98	-37.30	-74.77

E

Contribution	α-syn-VAPB
ΔEvdw	-276.4
ΔEele	-2368.92
ΔGpolar	2490.79
ΔGnonpolar	-30.43
ΔGtotal	-184.70

C

Contribution	VAPB-PTPIP51	p-α-syn-VAPB	p-α-syn-PTPIP51
ΔEvdw	-209.40	-119.61	-103.13
ΔEele	-752.23	-479.14	531.90
ΔGpolar	831.58	548.19	-464.50
ΔGnonpolar	-31.51	-16.69	-16.16
ΔGtotal	-161.55	-67.25	-51.90

F

Contribution	p-α-syn-VAPB
ΔEvdw	-287.53
ΔEele	-2196.95
ΔGpolar	2315.52
ΔGnonpolar	-32.31
ΔGtotal	-201.28

Fig. 3 The root mean square deviation (RMSD) plot of α-syn-VAPB-PTPIP51, mutant α-syn-VAPB-PTPIP51 (p-α-syn-VAPB-PTPIP51), α-syn-VAPB, and p-α-syn-VAPB systems **A**. A representative RMSD plot for α-syn-VAPB-PTPIP51 and p-α-syn-VAPB-PTPIP51 complexes. **B-C**. The binding free energy (in kcal/mol) and its components obtained from the MM/GBSA calculation for α-syn-VAPB-PTPIP51 (**B**) and p-α-syn-VAPB-PTPIP51 (**C**) complexes. **D**. A representative RMSD plot for α-syn-VAPB and p-α-syn-VAPB complexes. **E-F**. The binding free energy (in kcal/mol) and its components obtained from the MM/GBSA calculation for α-syn with VAPB (**E**) and p-α-syn with VAPB (**F**). The contribution to the binding free energy (ΔG_{total}) from the Van der Waals and electrostatic interactions is represented by ΔE_{vdw} and ΔE_{ele}, respectively. The polar and nonpolar solvation energy contributions to ΔG_{total} are represented by ΔGpolar and ΔGnonpolar, respectively

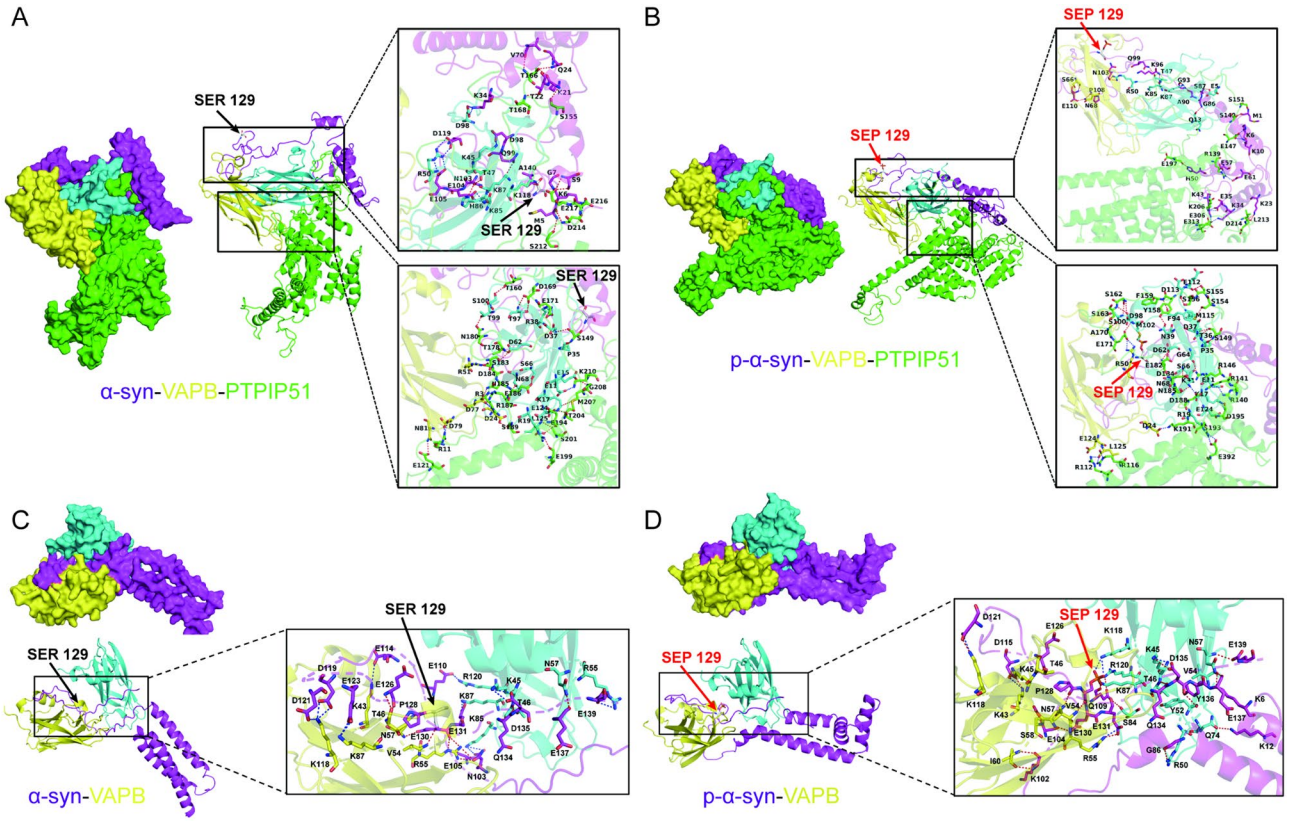

Fig. 4 Molecular dynamics (MD) simulations to explore the interaction mechanism of α-syn-VAPB-PTPIP51, mutant α-syn-VAPB-PTPIP51 (p-α-syn-VAPB-PTPIP51), α-syn-VAPB, and p-α-syn-VAPB systems. **A.** The interactions between VAPB and PTPIP51, α-syn and VAPB as well as α-syn and PTPIP51. **B.** The interactions between VAPB and PTPIP51, p-α-syn and VAPB as well as p-α-syn and PTPIP51. **C.** The interactions between α-syn and VAPB. **D.** The interactions between p-α-syn and VAPB. Chain A of VAPB (VAPB_A) is colored with cyan, Chain B of VAPB (VAPB_B) is colored with yellow. PTPIP51 is colored with green. α-syn and p-α-syn are colored with magenta. The key residues in VAPB_A are presented as cyan sticks. The key residues in VAPB_B are shown as yellow sticks. The key residues in PTPIP51 are shown as green sticks. The key residues in α-syn and p-α-syn are indicated by the magenta sticks. The red dashes represent hydrogen bond. The blue dashes represent salt bridge. The black arrows represent SER 129 site. The red arrows represent SEP 129 site

The extensive contact of p-α-syn along the VAPB-PTPIP51 interface could impact VAPB-PTPIP51 conformation and stability (Tables 1, 2, 3 and 4). To computationally address this phenomenon, we assessed the binding free energies among the α-syn-VAPB-PTPIP51 and p-α-syn-VAPB-PTPIP51 complexes. For the α-syn-VAPB-PTPIP51 complex, the binding free energies for the interactions of VAPB with PTPIP51, α-syn with VAPB, and α-syn with PTPIP51 were − 96.98, -37.30 and − 74.77 kcal/mol, respectively (Fig. 3B). On the other hand, for the p-α-syn-VAPB-PTPIP51 complex, the binding free energies for the interactions of VAPB with PTPIP51, p-α-syn with VAPB, and p-α-syn with PTPIP51 were − 161.55, -67.25 and − 51.90 kcal/mol, respectively (Fig. 3C). These findings suggest a better affinity between VAPB and PTPIP51 (-96.98 vs. -161.55) as well as between α-syn and the VAPB-PTPIP51 complex (-37.30 + -74.77 = -112.07 vs. -67.25 + -51.90 = -119.15), especially when residue SER129 mutates into residue SEP129 in α-syn. Moreover, these findings prove the reliability of our IP/MS and CO-IP results (Fig. 2).

Overall, our molecular docking experiments revealed that, in the α-syn-VAPB-PTPIP51 and p-α-syn-VAPB-PTPIP51 complexes, the VAPB-PTPIP51 binding interactions were more abundant in the p-α-syn-VAPB-PTPIP51 complex than in the α-syn-VAPB-PTPIP51 complex, leading to higher binding stability of VAPB and PTPIP51 in the former. The interaction residues in the 157–172 region (containing FFAT motif, 157-163AA) [41] were Thr160, Asp169, and Glu172 of PTPIP51 for the α-syn-VAPB-PTPIP51 complex, and Tyr158, Phe159, Ser162, Ser163, Ala170, and Glu171 for the p-α-syn-VAPB-PTPIP51 complex, indicating that VAPB could be stably embedded in the 157–172 region of PTPIP51 in the p-α-syn-VAPB-PTPIP51 complex. This could be the reason why α-syn can competitively interact with Thr166 and Thr168 to reduce interactions in the 157–172 region, whereas p-α-syn cannot. Furthermore, residues Pro108 and Glu110 of p-α-syn extended to interact with residues Ser66 and Asn68 of VAPB-B, forming a 'crab claw' structure that chelates with the VAPB dimer, increasing

Table 1 The contact list between VAPB and PTPIP51 in α-syn-VAPB-PTPIP51 complex

Chain	Residue	Chain	Residue	Interaction type
PTPIP51	Ser149.N	VAPB_A	Pro35.O	Hydrogen bond
PTPIP51	Ser149.O	VAPB_A	Asp37.N	Hydrogen bond
PTPIP51	Thr160.O	VAPB_A	Ser100.OG	Hydrogen bond
PTPIP51	Asp169.OD1/OD2	VAPB_A	Thr97.OG1/N	Hydrogen bond
PTPIP51	Glu171.OE2	VAPB_A	Arg38.NH1/NH2	Hydrogen bond, Salt bridge
PTPIP51	Thr178.OG1	VAPB_A	Asp62.OD1	Hydrogen bond
PTPIP51	Asn180.OD1	VAPB_A	Thr99.OG1	Hydrogen bond
PTPIP51	Ser183.OG	VAPB_A	Asp62.OD1	Hydrogen bond
PTPIP51	Glu186.OE2	VAPB_A	Ser66.OG	Hydrogen bond
PTPIP51	Arg187.N	VAPB_A	Asn68.OD1	Hydrogen bond
PTPIP51	Glu194.OE2	VAPB_A	Lys17.NZ	Hydrogen bond, Salt bridge
PTPIP51	Glu199.O	VAPB_A	Arg19.NH1	Hydrogen bond
PTPIP51	Ser201.OG	VAPB_A	Leu125.N/OC2	Hydrogen bond
PTPIP51	Thr204.OG1	VAPB_A	Glu124.OE1	Hydrogen bond
PTPIP51	Met207.SD	VAPB_A	Lys17.CE	Hydrogen bond
PTPIP51	Gly208.N	VAPB_A	Glu15.OE2	Hydrogen bond
PTPIP51	Lys210.NZ	VAPB_A	Glu11.OE1	Hydrogen bond, Salt bridge
PTPIP51	Arg3.NE/NH2	VAPB_B	Asp77.OD2	Hydrogen bond, Salt bridge
PTPIP51	Arg11.NH2/NH1	VAPB_B	Asp79.OD1/OD2	Hydrogen bond, Salt bridge
PTPIP51	Glu121.OE2	VAPB_B	Asn81.ND2	Hydrogen bond
PTPIP51	Asp184.OD1/OD2	VAPB_B	Arg51.NH2/NH1	Hydrogen bond, Salt bridge
PTPIP51	Asn185.ND2	VAPB_B	Asp77.OD1	Hydrogen bond
PTPIP51	Arg187.NH1/NH2	VAPB_B	Asp77.OD2/OD1	Hydrogen bond, Salt bridge
PTPIP51	Ser189.OG	VAPB_B	Asp24.OD1	Hydrogen bond

Table 2 The contact list between α-syn and VAPB as well as α-syn and PTPIP51 in α-syn-VAPB-PTPIP51 complex

Chain	Residue	Chain	Residue	Interaction type
PTPIP51	Ser155.O	α-syn	Lys21.CE	Hydrogen bond
PTPIP51	Thr166.OG1	α-syn	Lys21.O	Hydrogen bond
PTPIP51	Thr166.OG1	α-syn	Gln24.NE2	Hydrogen bond
PTPIP51	Thr166.N	α-syn	Val70.O	Hydrogen bond
PTPIP51	Thr168.N	α-syn	Thr22.OG1	Hydrogen bond
PTPIP51	Ser212.O	α-syn	Met5.N	Hydrogen bond
PTPIP51	Asp214.N	α-syn	Met5.O	Hydrogen bond
PTPIP51	Asp214.OD2	α-syn	Lys6.NZ	Hydrogen bond, Salt bridge
PTPIP51	Glu216.OE1	α-syn	Lys6.NZ	Hydrogen bond, Salt bridge
PTPIP51	Glu217.OE2	α-syn	Gly7.N	Hydrogen bond, Salt bridge
PTPIP51	Glu217.OE2	α-syn	Ser9.N/OG	Hydrogen bond
VAPB_A	Lys45.NZ	α-syn	Asp98.OD1	Hydrogen bond, Salt bridge
VAPB_A	Thr47.OG1	α-syn	Asn103.OD1	Hydrogen bond
VAPB_A	Arg50.NE/NH2	α-syn	Glu105.OE1/OE2	Hydrogen bond, Salt bridge
VAPB_A	Arg50.NH1/NH2	α-syn	Asp119.OD1/OD2	Hydrogen bond, Salt bridge
VAPB_A	Lys85.O	α-syn	Asn103.ND2	Hydrogen bond
VAPB_A	Lys85.NZ	α-syn	Glu104.OE1/OE2	Hydrogen bond, Salt bridge
VAPB_A	His86.ND1	α-syn	Asn103.OD1	Hydrogen bond
VAPB_A	Lys87.CE	α-syn	Gln99.OE1	Hydrogen bond
VAPB_A	Asp98.OD1/OD2	α-syn	Lys34.NZ	Hydrogen bond, Salt bridge
VAPB_A	Lys118.NZ	α-syn	Ala140.OC2	Hydrogen bond, Salt bridge

Table 3 The contact list between VAPB and PTPIP51 in p-α-syn-VAPB-PTPIP51 complex

Chain	Residue	Chain	Residue	Interaction type
PTPIP51	Arg140.NH2	VAPB_A	Glu11.OE1	Hydrogen bond
PTPIP51	Arg141.NH2	VAPB_A	Glu11.OE1	Hydrogen bond
PTPIP51	Arg146.NH2	VAPB_A	Gly64.O	Hydrogen bond
PTPIP51	Ser149.N	VAPB_A	Pro35.O	Hydrogen bond
PTPIP51	Ser149.O	VAPB_A	Thr36.CA	Hydrogen bond
PTPIP51	Ser149.O	VAPB_A	Asp37.N	Hydrogen bond
PTPIP51	Ser154.OG	VAPB_A	Met115.SD	Hydrogen bond
PTPIP51	Ser155.OG	VAPB_A	Glu112.O	Hydrogen bond
PTPIP51	Ser156.OG	VAPB_A	Asp113.O	Hydrogen bond
PTPIP51	Tyr158.OH	VAPB_A	Asn39.OD1	Hydrogen bond
PTPIP51	Phe159.N	VAPB_A	Phe94.O	Hydrogen bond
PTPIP51	Ser162.N	VAPB_A	Asp98.O	Hydrogen bond
PTPIP51	Ser162.OG	VAPB_A	Ser100.N	Hydrogen bond
PTPIP51	Ser163.N	VAPB_A	Asp98.O	Hydrogen bond
PTPIP51	Ala170.N	VAPB_A	Ser100.O	Hydrogen bond
PTPIP51	Glu171.OE1	VAPB_A	Met102.N	Hydrogen bond, Salt bridge
PTPIP51	Glu182.N	VAPB_A	Asp62.OD1	Hydrogen bond
PTPIP51	Asp184.OD1	VAPB_A	Ser66.N/OG	Hydrogen bond, Salt bridge
PTPIP51	Asn185.OD1	VAPB_A	Lys31.NZ	Hydrogen bond
PTPIP51	Asn185.OD1	VAPB_A	Asn68.ND2	Hydrogen bond, Salt bridge
PTPIP51	Asp188.OD2	VAPB_A	Lys31.NZ	Hydrogen bond, Salt bridge
PTPIP51	Ser193.O	VAPB_A	Arg19.NH1	Hydrogen bond, Salt bridge
PTPIP51	Asp195.OD1/OD2	VAPB_A	Lys17.NZ	Hydrogen bond, Salt bridge
PTPIP51	Asp195.N	VAPB_A	Glu124.OE1	Hydrogen bond, Salt bridge
PTPIP51	Glu392.OE1/OE2	VAPB_A	Arg19.NH1/NH2	Hydrogen bond, Salt bridge
PTPIP51	Arg112.OE1/OE2	VAPB_A	Glu124.NH2/NH1	Hydrogen bond
PTPIP51	Arg112.NH2/NH1	VAPB_B	Leu125.OC1	Hydrogen bond
PTPIP51	Arg116.NH2/NE	VAPB_B	Leu125.OC1/OC2	Hydrogen bond
PTPIP51	Glu171.OE2	VAPB_B	Arg50.NH1/NH2	Hydrogen bond
PTPIP51	Lys191.NZ	VAPB_B	Asp24.OD2	Hydrogen bond
PTPIP51	Arg140.NH2	VAPB_B	Glu11.OE1	Hydrogen bond

the stability of the interaction between p-α-syn and the VAPB-PTPIP51 complex.

Phosphorylation at the serine 129 site of α-syn influenced the dynamics of the α-syn-VAPB and α-syn-PTPIP51 complexes

In 2024, Christopher J. Obara and colleagues employed three-dimensional electron microscopy combined with high-speed molecular tracking to study VAPB. Their findings revealed that VAPB molecules transiently enter and exit ER-mitochondrial contact sites within seconds, while the contact sites themselves remain stable over significantly longer time scales [39]. Based on these observations, we propose that, in addition to their role in tethering ER and mitochondria, VAPB and PTPIP51 proteins may also have distinct functions in both physiological and pathological contexts. Therefore, we conducted additional experiments to investigate the binding interactions of p-α-syn with VAPB and PTPIP51 individually, in comparison to the interactions observed with α-syn. We focused on VAPB, which is notably expressed in mouse midbrain (Supplementary Material. Figure 3 C). RMSD analysis indicates that both the α-syn-VAPB and p-α-syn-VAPB systems reached equilibrium within the simulation timeframe (Fig. 3B). Furthermore, RMSF analysis demonstrates that the protein exhibited fluctuations within an acceptable range (Supplementary Material. Figure 4E-G). Figure 4 C-D illustrate the binding configurations of the α-syn-VAPB and p-α-syn-VAPB complexes. The contact interactions for these complexes are detailed in Tables 5 and 6. We also assessed the binding free energy among the α-syn-VAPB and p-α-syn-VAPB complexes. The average binding free energies for the interactions of α-syn with VAPB, p-α-syn with VAPB were – 184.70 and – 201.28 kcal/mol, respectively (Fig. 3E-F). Additionally, we employed AlphaFold3 to predict the complex structures of α-syn-PTPIP51 and p-α-syn-PTPIP51. The binding configurations and contact interactions for α-syn with PTPIP51 and p-α-syn with PTPIP51 are presented in the Supplementary Material. Figure 5.

According to the MD results, we found the p-α-syn-VAPB complex exhibits a more extensive and intricate

Table 4 The contact list between p-α-syn and VAPB as well as p-α-syn and PTPIP51 in p-α-syn-VAPB-PTPIP51 complex

Chain	Residue	Chain	Residue	Interaction type
PTPIP51	Arg139.NH2/NE	p-α-syn	Glu57.OE2	Hydrogen bond, Salt bridge
PTPIP51	Arg139.NH2	p-α-syn	Glu61.OE1	Hydrogen bond, Salt bridge
PTPIP51	Glu147.OE2	p-α-syn	Lys6.NZ	Hydrogen bond, Salt bridge
PTPIP51	Glu147.OE1/OE2	p-α-syn	Lys10.NZ	Hydrogen bond, Salt bridge
PTPIP51	Ser149.OG	p-α-syn	Met1.O	Hydrogen bond
PTPIP51	Ser151.OG	p-α-syn	Met1.N	Hydrogen bond
PTPIP51	Glu197.O	p-α-syn	His50.NE2	Hydrogen bond
PTPIP51	Lys206.NZ	p-α-syn	Glu35.OE1/OE2	Hydrogen bond, Salt bridge
PTPIP51	Leu213.O	p-α-syn	Lys23.NZ	Hydrogen bond
PTPIP51	Asp214.O	p-α-syn	Lys23.NZ	Hydrogen bond
PTPIP51	Glu306.OE2	p-α-syn	Lys34.NZ	Hydrogen bond, Salt bridge
PTPIP51	Glu313.OE2	p-α-syn	Lys43.NZ	Hydrogen bond, Salt bridge
VAPB_A	Glu5.OE1	p-α-syn	Ser87.OG	Hydrogen bond
VAPB_A	Gln13.O	p-α-syn	Gly86.N	Hydrogen bond
VAPB_A	Thr47.O	p-α-syn	Gln99.NE2	Hydrogen bond
VAPB_A	Arg50.NH1/NH2	p-α-syn	Asn103.O	Hydrogen bond
VAPB_A	Lys85.O	p-α-syn	Lys96.N	Hydrogen bond
VAPB_A	Lys87.NZ	p-α-syn	Ala90.O	Hydrogen bond
VAPB_A	Lys87.NZ	p-α-syn	Gly93.O	Hydrogen bond
VAPB_B	Ser66.O	p-α-syn	Glu110.N	Hydrogen bond
VAPB_B	Asn68.ND2	p-α-syn	Pro108.O	Hydrogen bond
VAPB_B	Asn68.ND2	p-α-syn	Glu110.OE1	Hydrogen bond

interaction than the α-syn-VAPB complex. The p-α-syn protein undergoes a more pronounced conformational change compared to α-syn, resulting in a significantly enhanced interaction between its C-terminal and VAPB. Specifically, SER129 of α-syn forms an intermolecular hydrogen bond with Val54 of VAPB_B, whereas SEP129 of p-α-syn can establish both hydrogen bonds and salt bridge interactions with Lys118 and Lys87 of adjacent VAPB_A due to its longer side chain. Furthermore, the region spanning Leu100 to Gly133 in p-α-syn presents a broader contact area with VAPB_B compared to α-syn, thereby facilitating increased interactions between p-α-syn and VAPB. This leads to a more rapid attainment of a stable state during MD simulations. The lower binding free energy associated with the substitution of SER129 in α-syn with SEP129 indicates that p-α-syn exhibits a higher affinity for VAPB.

Identification and functional annotation of the VAPB and p-α-syn common interacting proteins in the midbrain of Thy1-SNCA transgenic mice

Based on the aforementioned CO-IP and MD simulation analysis results, we speculated that VAPB interacted mainly with the C-terminus of α-syn (90-140AA), with or without phosphorylation at the serine 129 site [42]. Nonetheless, the functional roles of these interactions remain unclear. Among the genes identified to carry *de novo* mutations, various data sources have supported the involvement of VAPB in PD, with one study reporting a *de novo* in-frame deletion of a valine residue at position 25 (p.ΔV25) in VAPB in an independent cohort of sporadic PD cases [22]. To further establish whether α-syn overexpression or its interactions would affect VAPB function in a pathological state, we performed CO-IP/MS experiments to identify the VAPB interacting proteins in the midbrain of Wt and Tg mice. Protein complexes were pulled down and detected via WB using the VAPB antibody (Proteintech, 14477-1-AP). According to the results, the antibodies significantly enriched VAPB compared to non-immune IgG controls (Fig. 5A-B). Subsequently, we subjected the IP protein complexes to electrophoresis and confirmed them via in-gel digestion and proteomics analyses. Our IP/MS identified 92 and 107 proteins (Peptides 95% ≥ 1) as putative binding partners of VAPB in the Wt and Tg groups, respectively (Fig. 5C, Supplementary Material. Table 10 and 11). Considering the intersections of the p-α-syn and VAPB interacting proteins, we identified 53 proteins as high-confidence common interacting proteins of p-α-syn and VAPB (Fig. 5D, Supplementary Material. Table 7).

To further understand the physiological processes underlying the interactions of p-α-syn and VAPB, we uploaded the candidate 53 proteins of interest to DAVID (http://david.abcc.ncifcrf.gov/) for functional annotation. The top 10 GO terms for Biological Processes (BPs; Fig. 6A), Cellular Components (CCs, Fig. 6B), and Molecular Functions (MFs; Fig. 6C) were then listed. According to the GO enrichment analysis results, the common

Table 5 The contact list between α-syn and VAPB in α-syn-VAPB complex

Chain	Residue	Chain	Residue	Interaction type
α-syn	GLU105.OE1/OE2	VAPB_A	LYS85.NZ	Hydrogen bond, Salt bridge
α-syn	GLU110.OE1	VAPB_A	ARG120.NH2	Hydrogen bond, Salt bridge
α-syn	GLU131.OE1/OE2	VAPB_A	LYS87.NZ	Hydrogen bond, Salt bridge
α-syn	GLN134.N	VAPB_A	THR46.O	Hydrogen bond
α-syn	GLN134.O	VAPB_A	THR46.N	Hydrogen bond
α-syn	ASP135.OD1/OD2	VAPB_A	LYS45.NZ	Hydrogen bond, Salt bridge
α-syn	GLU137.O	VAPB_A	ASN57.ND2	Hydrogen bond
α-syn	GLU139.OE1	VAPB_A	ARG55.NH2	Hydrogen bond, Salt bridge
α-syn	GLU139.OE1/OE2	VAPB_A	ARG55.NE	Hydrogen bond
α-syn	ASN103.OD1	VAPB_B	ARG55.NH1/NH2	Hydrogen bond
α-syn	GLU114.OE2	VAPB_B	LYS43.NZ	Salt bridge
α-syn	ASP119.OD1/OD2	VAPB_B	LYS118.NZ	Hydrogen bond, Salt bridge
α-syn	ASP121.OD2	VAPB_B	LYS118.NZ	Hydrogen bond, Salt bridge
α-syn	GLU123.OE1/OE2	VAPB_B	LYS87.NZ	Hydrogen bond, Salt bridge
α-syn	GLU126.N	VAPB_B	THR46.O	Hydrogen bond
α-syn	GLU126.O	VAPB_B	THR46.N	Hydrogen bond
α-syn	PRO128.O	VAPB_B	ASN57.ND2	Hydrogen bond
α-syn	SER129.O	VAPB_B	VAL54.N	Hydrogen bond
α-syn	GLU130.OE1	VAPB_B	ASN57.N	Hydrogen bond
α-syn	GLU130.O	VAPB_B	ARG55.NE/NH2	Hydrogen bond

interacting proteins of p-α-syn and VAPB significantly involved in various fundamental processes including protein binding, metal ion binding, structural constituent of the cytoskeleton, intermediate filament cytoskeleton, and microtubule organization pathways, among others. On the other hand, the KEGG analysis results demonstrated that the common interacting proteins of p-α-syn and VAPB were mainly enriched in various PD-related and neurodegeneration pathways, including multiple diseases, prion diseases, and PD (Fig. 6D), suggesting that these proteins could be crucially involved in the pathogenicity of PD.

Verification of the downstream proteins interacted with VAPB and p-α-syn.

To further identify the proteins that mediate the synergistic effects of p-α-syn and VAPB, we compared VAPB interacting proteins in the midbrains of Wt and Tg mice. Our MS analysis identified 53 proteins as partners of both p-α-syn and VAPB in the midbrain of Tg mice. Notably, only 15 of these proteins were unique to the Tg group and were absent in Wt group (Fig. 7A, Supplementary material. Table 7). The functions of these 15 proteins were annotated using the DAVID bioinformatics resources. According to KEGG pathway enrichment analysis results, the 15 interacting candidates were mainly enriched in four pathways, including the synaptic vesicle cycle (NSF/STXBP1/CLTC/SLC1A3/DNM1), calcium reabsorption (CLTC/ATP1A3/DNM1), Huntington disease (CLTC/SLC1A3/VDAC1/TUBB4B), and bacterial invasion of epithelial cells (CLTC/DNM1) (Fig. 7B). We performed WB analysis to quantify the protein levels of CLTC (Clathrin Heavy Chain 1), TUBB4B (Tubulin β-4B chain), PTPIP51, CAMK2A (Calcium/Calmodulin-dependent Protein Kinase Type II Subunit α), and ATP1A3 (Sodium/potassium-transporting ATPase subunit α-3) in the midbrain of Wt and Tg mice (Supplementary material. Figure 3E-H). Based on these results, we conducted CO-IP experiments to explore the interactions among the target proteins. Our findings confirmed the interaction between p-α-syn and CLTC (Fig. 7C), CLTC and VAPB (Fig. 7D), VAPB and p-α-syn, VAPB and PTPIP51 (Fig. 7E), VAPB and TUBB4B (Fig. 7F), VAPB and CLTC, VAPB and CAMK2A (Fig. 7G), VAPB and ATP1A3 (Fig. 7H) in the midbrain of Tg mice.

Discussion

Although α-syn phosphorylation occurs at the serine 129 site in Lewy pathology, the drivers of this phosphorylation and the exact composition of Lewy bodies (LBs) remain unclear [43]. Therefore, further studies should identify molecules mediating the functional interaction with α-syn and the mechanism by which phosphorylation at the serine 129 site of α-syn exerts its regulatory function in pathological situations. In this study, p-α-syn was detected in the midbrains of Thy1-SNCA transgenic mice using one specific p-α-syn antibody (CST, #23706), followed by CO-IP/MS analysis. Unlike h-α-syn, unexpected divergence was detected in p-α-syn interacting proteins. However, we focused on VAPB-PTPIP51,

Table 6 The contact list between p-α-syn and VAPB in p-α-syn-VAPB complex

Chain	Residue	Chain	Residue	Interaction type
p-α-syn	LYS6.NZ	VAPB_A	VAL54.O	Hydrogen bond
p-α-syn	LYS12.NZ	VAPB_A	GLN74.OE1	Hydrogen bond
p-α-syn	GLY86.O	VAPB_A	ARG50.NH2	Hydrogen bond
p-α-syn	GLY109.OE1	VAPB_A	ARG120.NH1	Hydrogen bond
p-α-syn	GLY109.NE2	VAPB_A	SER84.O	Hydrogen bond
p-α-syn	GLY109.O	VAPB_A	LYS87.NZ	Hydrogen bond
p-α-syn	SEP129.O8/O9	VAPB_A	LYS118.NZ	Hydrogen bond, Salt bridge
p-α-syn	SEP129.O10	VAPB_A	LYS87.NZ	Hydrogen bond, Salt bridge
p-α-syn	GLN134.N	VAPB_A	THR46.O	Hydrogen bond
p-α-syn	GLN134.O	VAPB_A	THR46.N	Hydrogen bond
p-α-syn	ASP135.OD1/OD2	VAPB_A	LYS45.NZ	Hydrogen bond, Salt bridge
p-α-syn	TYR136.OH	VAPB_A	TYR52.O	Hydrogen bond
p-α-syn	GLU137.O	VAPB_A	ASN57.ND2	Hydrogen bond
p-α-syn	GLU139.OE2	VAPB_A	ASN57.N	Hydrogen bond
p-α-syn	LYS102.O	VAPB_B	ILE60.N	Hydrogen bond
p-α-syn	LYS102.N	VAPB_B	ILE60.O	Hydrogen bond
p-α-syn	GLU104.OE1	VAPB_B	SER58.OG	Hydrogen bond
p-α-syn	ASP115.OD1/OD2	VAPB_B	LYS43.NZ	Hydrogen bond, Salt bridge
p-α-syn	ASP115.OD2	VAPB_B	LYS45.NZ	Hydrogen bond, Salt bridge
p-α-syn	ASP121.OD1/OD2	VAPB_B	LYS118.NZ	Hydrogen bond, Salt bridge
p-α-syn	GLU126.N	VAPB_B	THR46.O	Hydrogen bond
p-α-syn	GLU126.O	VAPB_B	THR46.N	Hydrogen bond
p-α-syn	PRO128.O	VAPB_B	ASN57.ND2	Hydrogen bond
p-α-syn	GLU130.OE2	VAPB_B	ASN57.N	Hydrogen bond
p-α-syn	GLU131.OE1/OE2	VAPB_B	ARG55.NH2	Hydrogen bond, Salt bridge

one pair of ER-mitochondria tethers in MAMs, of the 56 potential interacting proteins (specifically with p-α-syn). CO-IP and MD simulation results further confirmed that the phosphorylation at the serine 129 site of α-syn increased the interaction between VAPB and PTPIP51, α-syn and VAPB. Moreover, molecular docking results showed that, α-syn-VAPB interactions and α-syn-PTPIP51 interactions were mainly mediated by the C-terminus of α-syn (90-140AA) and the N-terminus of α-syn (1-60AA), respectively, with or without phosphorylation at serine 129 site. Furthermore, key downstream pathways shared by p-α-syn and VAPB, including protein binding, metal ion binding, structural constituent of cytoskeleton, intermediate filament cytoskeleton and microtubule organization pathways, etc., were identified. Overall, the findings confirm that the phosphorylation at the serine 129 site of α-syn plays a key role in regulating the protein interactome, providing possible mechanisms by which p-α-syn and VAPB participate in α-syn pathogenesis.

Researchers have recently utilized new techniques with AlphaFold driven modeling and membrane-binding simulations, and found that phosphorylation at the serine 129 site can induce conformational changes. Besides, this phosphorylation can trigger protein-protein interactions, which are necessary for mediating α-syn function at the synapse [12]. Although numerous studies have directly used p-α-syn antibodies in histology and immunoblot techniques to detect the progression of α-syn pathology in PD [12, 44, 45], most commercially available p-α-syn antibodies cannot be used in CO-IP experiment. Also, some p-α-syn antibodies can cross-react with nonspecific antigens, thus limiting the study of p-α-syn interacting proteins [46, 47]. In previous studies, pulled-down protein complexes between non-phosphorylated α-syn C-terminus and serine 129 site phosphorylated α-syn C-terminus have been investigated using the combination of peptide pulldown/MS assays [14]. In addition, another study labeled total α-syn (Abcam, ab138501) and p-α-syn (Abcam, ab51253) in situ using a technique called biotinylation by antibody recognition for subsequent MS analysis of brain tissues [15, 16]. In the present study, CO-IP/MS was directly conducted with h-α-syn antibody (Abcam, ab138501) and p-α-syn antibody (CST, #23706). The two antibodies showed high specificity and affinity towards h-α-syn and p-α-syn in mouse brains. Moreover, the MS results identified 205 and 225 proteins (Peptides 95% ≥ 2) as putative binding partners of h-α-syn and p-α-syn, respectively (in the midbrain of 13-month-old Tg mice) (Supplementary material, Table 8 and 9). These results are consistent with the conclusion that h-α-syn and p-α-syn interacting proteins are different. Therefore, this study provides a valuable tool for subsequent CO-IP studies of h-α-syn and p-α-syn, and may

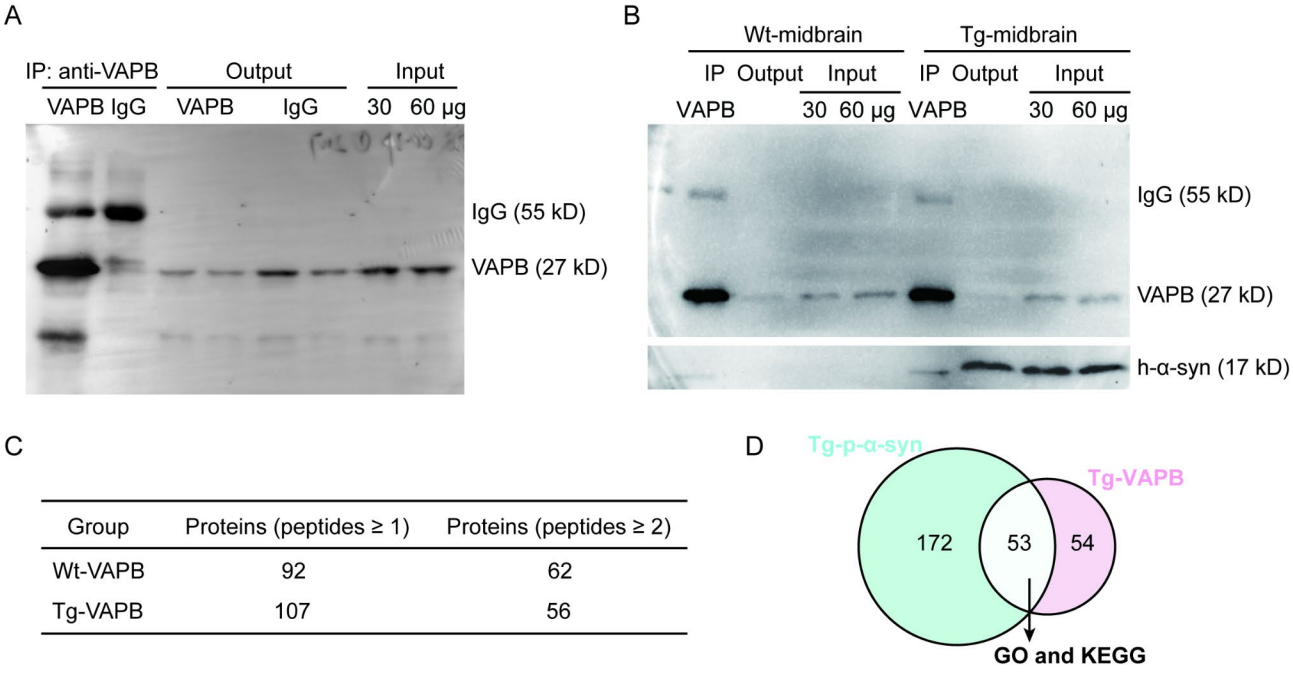

Group	Proteins (peptides ≥ 1)	Proteins (peptides ≥ 2)
Wt-VAPB	92	62
Tg-VAPB	107	56

Fig. 5 Identification of VAPB interacting proteins in the midbrain of Thy1-SNCA transgenic mice and Wild-type mice through LC-MS/MS **A-B**. WB analysis of proteins immunoprecipitated with VAPB in the midbrain of Tg mice (**A-B**) and Wt mice (**B**). **C**. Proteins identified with a minimum of 1 unique peptide (Peptides 95% ≥ 1) were included in analyses (Supplementary material. Table 10 and 11). **D**. Venn diagrams depicting the degree of overlap in numbers of proteins which differentially interacted with the p-α-syn (Peptides 95% ≥ 2) and VAPB (Peptides 95% ≥ 1) in the midbrain of Tg mice. The gray area showing the common proteins interacting with p-α-syn and VAPB (includes 53 proteins, Supplementary material. Table 7). The 53 proteins of interest were uploaded to the DAVID to perform GO analysis and KEGG pathway enrichment. VAPB was analyzed with VAPB antibody (Proteintech, 14477-1-AP). The midbrain homogenates derived from 13 months-old Wt and Tg mice, normal rabbit IgG served as the negative control. Venn diagram was plotted by https://www.bioinformatics.com.cn (last accessed on 20 June 2024), an online platform for data analysis and visualization.

help clarify the regulatory mechanism of phosphorylation at the serine 129 site of α-syn.

VAPB is a highly conserved integral membrane protein in the ER that facilitates the anchoring of membranous organelles to the ER [21]. Previous immunoelectron microscopy revealed that α-syn and VAPB are localized to filamentous structures of LBs in PD [48]. Additionally, several studies have shown that VAPB is involved in PD progression, and may be associated with the formation of vesicular structures and LBs [22, 48, 49]. In the present study, CO-IP/MS identified VAPB as a putative binding partner in p-α-syn interacting group in the midbrain of 13-month-old Tg mice. CO-IP and MD simulation assays confirmed this finding. The differential interaction illustrates for the first time that phosphorylation at the serine 129 site of α-syn increases the interaction between α-syn and VAPB. Previous studies reported that α-syn directly binds to the MSP domain of VAPB, resulting in the disruption of calcium ion homeostasis and mitochondrial ATP production [23]. Herein, MD findings showed that the MSP domain of VAPB mainly interacted with the C-terminus of α-syn (90-140AA), with or without phosphorylation at serine 129 of α-syn. However, further research is needed to validate α-syn-VAPB interacting regions via GST-pull-down assays.

Furthermore, literature has established that MAMs dysfunction is closely related to PD pathogenesis, thereby affecting the communication between ER and mitochondria [50, 51]. VAPB-PTPIP51 tethering complex localizes in MAMs and forms at least one scaffold that mediates ER-mitochondria associations [18]. A recent study further indicated that VAPB is significantly correlated with the metastability of MAMs [39]. Additionally, Wild-type α-syn and its PD-associated mutants A30P and A53T can interact with the VAPB-PTPIP51 tethering complex, thus influencing MAMs dynamics [23, 52]. The above studies provide innovative research direction for exploring the detailed molecular mechanisms of α-syn and VAPB-PTPIP51 in regulating MAMs functions in α-syn pathogenesis. In this study, the CO-IP/MS results ordered the potential interacting proteins (specifically with p-α-syn) based on peptide spectrum matches and coverage percentage, PTPIP51 ranked first (Supplementary material. Table 7). The only study that conducted related analysis using IP assay of PTPIP51 and h-α-syn co-transfected HEK293 cells did not detect any interaction between α-syn and PTPIP51 [23]. Unlike previous research, IP results in SHSY5Y cells showed the interaction between α-syn and PTPIP51, with or without phosphorylation at the serine 129 site of α-syn. Notably, both MD

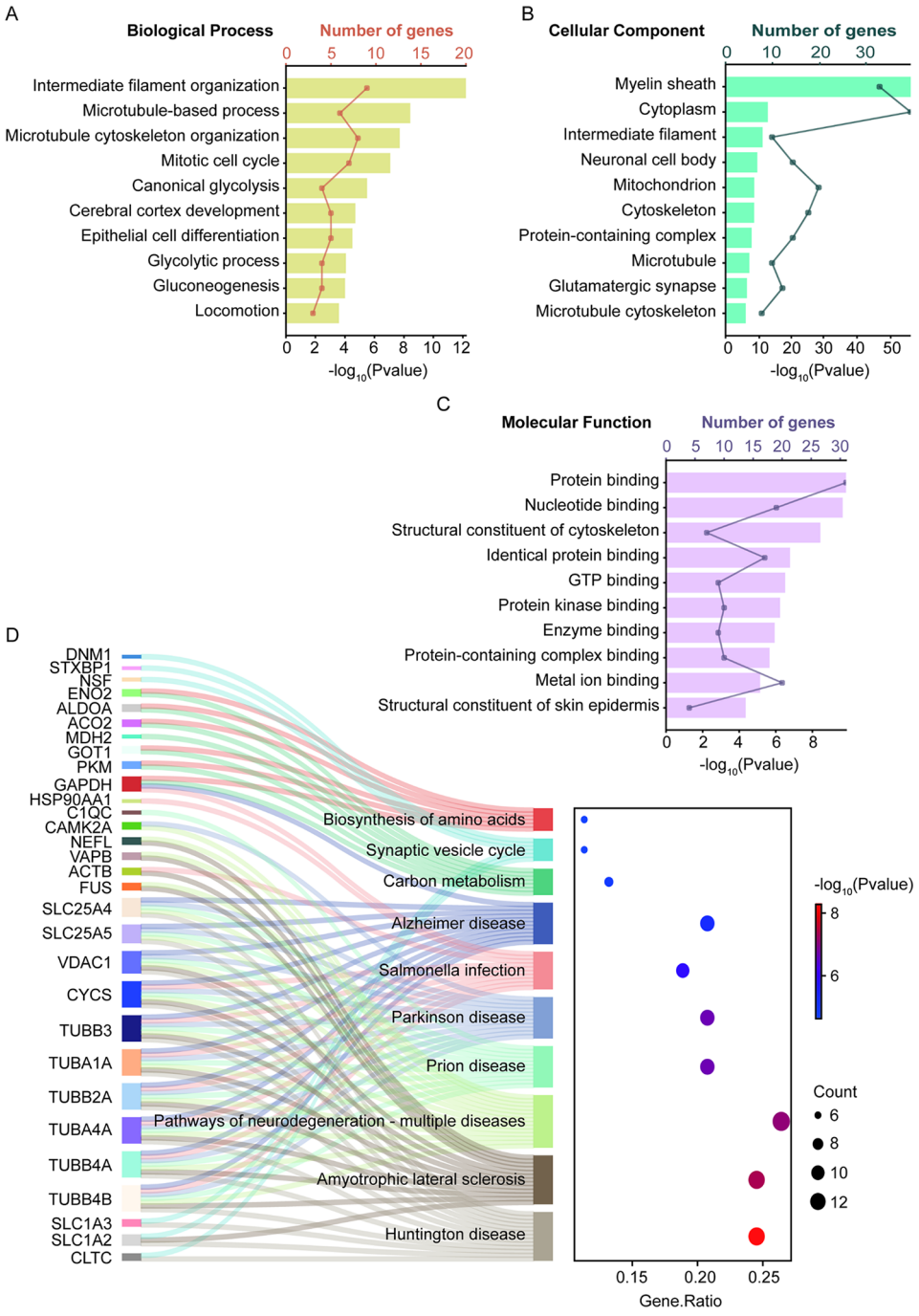

Fig. 6 GO and KEGG pathway analysis of p-α-syn-VAPB interacting proteins in the midbrain of Thy1-SNCA transgenic mice **A-D**. GO and KEGG enrichment analysis on the DAVID database. The top 10 GO terms in the biological process (**A**), cellular component (**B**), and molecular function (**C**) are listed. Top 10 KEGG signaling pathways (**D**) are listed. GO, gene ontology; KEGG, Kyoto encyclopedia of genes and genomes

simulations and AlphaFold3 predictive results demonstrated that the interactions between α-syn and PTPIP51 are predominantly facilitated by the N-terminal region of α-syn (1-60AA). Besides, there was a lower affinity between α-syn and PTPIP51 (-74.77 vs. -51.90 kcal/mol) when residue SER129 mutated into residue SEP129 in α-syn, inconsistent with MS and CO-IP results. Several studies have confirmed the interaction between VAPB and PTPIP51. Consequently, VAPB may serve as an intermediary in the interaction between α-syn and PTPIP51, as no direct interaction between α-syn and PTPIP51 has been documented. Furthermore, the interactions between α-syn and PTPIP51 are modulated by the phosphorylation of α-syn at the serine residue 129 [53].

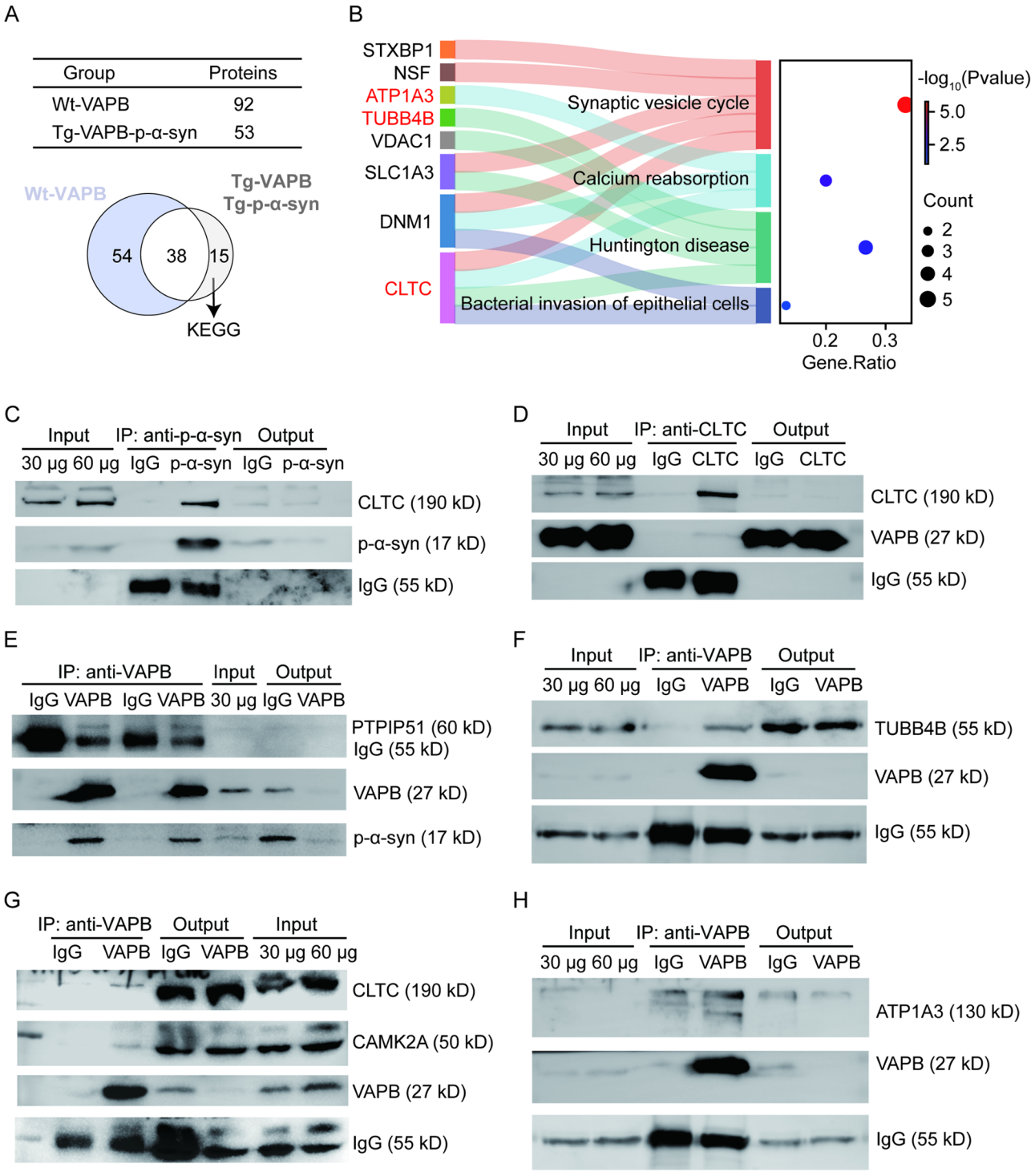

Fig. 7 The immunoprecipitation assay confirming the interaction between p-α-syn-VAPB and identification of their interacting proteins through LC-MS/MS. **A.** Venn diagrams displaying the degree of overlap in numbers of proteins which differentially interacted with VAPB in Wt mice (Peptides 95% ≥ 1, includes 92 proteins) and p-α-syn-VAPB in Tg mice (includes 53 proteins). The grey area displays proteins interacting with p-α-syn and VAPB in midbrain of Tg mice (includes 15 proteins). **B.** KEGG pathway enrichment for 15 differentially interacted proteins. **C**-**H.** CO-IP analysis of the interaction between p-α-syn and CLTC (**C**), CLTC and VAPB (**D**), VAPB and p-α-syn, VAPB and PTPIP51 (**E**), VAPB and TUBB4B (**F**), VAPB and CLTC, VAPB and CAMK2A (**G**), VAPB and ATP1A3 (**H**). IP antibody: anti-p-α-syn (CST, #23706), anti-VAPB (Proteintech, 14477-1-AP), and anti-CLTC (Proteintech, 26523-2-AP). CLTC, Clathrin Heavy Chain 1. ATP1A3, Sodium/potassium-transporting ATPase subunit α-3. CAMK2A, Calcium/Calmodulin-dependent Protein Kinase type II subunit α. TUBB4B, Tubulin β-4B chain. The midbrain homogenates were from 13 months-old Tg mice, normal rabbit IgG served as the negative control

Nonetheless, GST-pull-down assays are needed to detect any direct interaction between α-syn and PTPIP51, as well as the interacting regions.

The mechanism underlying α-syn in MAMs is controversial. Some studies have reported that α-syn controls mitochondrial calcium homeostasis by enhancing ER-mitochondria interactions [54]. However, another study reported that α-syn can induce the loosening of ER-mitochondria contacts, accompanied by disruption to calcium ions exchange between the two organelles and mitochondrial ATP production [23]. In this study, molecular docking experiments indicated that VAPB and PTPIP51 had more abundant interactions in p-α-syn-VAPB-PTPIP51 than in α-syn-VAPB-PTPIP51, leading to higher binding stability between VAPB and PTPIP51 in p-α-syn-VAPB-PTPIP51 (-96.98 vs. -161.55 kcal/mol). Taken together, these finding indicate that α-syn enhances ER-mitochondria interaction, however, further validation is required. Furthermore, molecular docking experiments showed that the MSP domain of VAPB can be embedded stably in 157–172 region (FFAT-like motif) of PTPIP51 in α-syn-VAPB-PTPIP51 and p-α-syn-VAPB-PTPIP51 complexes, consistent with previously studies [25, 55].

Previous studies have shown that α-syn and VAPB are involved in PD progression, and may be associated with the formation of α-syn pathogenesis [48, 49]. In the present study, GO enrichment analysis demonstrated that 53 high-confidence p-α-syn and VAPB common interacting proteins were significantly involved in many fundamental processes, including structural constituent of cytoskeleton, protein binding, protein kinase binding, protein-containing complex binding pathways, etc. This was partly consistent with previous peptide pulldown and MS research. Previous research found that α-syn peptide phosphorylation at the serine 129 site is highly enriched in certain cytoskeletal proteins, vesicular trafficking proteins, and some enzymes [14]. Herein, CO-IP results showed that p-α-syn could bind to VAPB and TUBB4B (Tubulin β-4B chain). Furthermore, the interactions between p-α-syn/VAPB and CLTC (Clathrin Heavy Chain 1) were verified. These interactions are involved in autophagosome formation [38, 56, 57]. These findings confirm that LBs formation involves a complex interplay between α-syn fibrillization and posttranslational modifications, as well as interactions between α-syn aggregates and membranous organelles [58, 59].

Additionally, VAPB interacting proteins were different between Wt and Tg groups, suggesting the impact of α-syn overexpression and phosphorylation at the serine 129 site of α-syn on the downstream functions of VAPB (Supplementary material. Table 10 and 11). Functional enrichment analysis of the screened 15 proteins interacting specifically with p-α-syn and VAPB in the Tg group, showed that the proteins were mainly enriched in four pathways, including synaptic vesicle cycle (NSF/STXBP1/CLTC/SLC1A3/DNM1) and calcium reabsorption (CLTC/ATP1A3/DNM1), as the top two pathways. Consistently, previous studies reported that the impairment of VAPB-PTPIP51 tethering activity is associated with MAMs dysfunctions, including cellular calcium ions homeostasis imbalance and neuronal synaptic dysfunction [23, 60, 61]. Moreover, studies have shown that VAPB and phosphorylation at the serine 129 site of α-syn participate in the regulation of synaptic vesicle cycle and presynaptic calcium ions homeostasis [12, 62]. In this study, CO-IP identified the interaction between VAPB and ATP1A3 (Sodium/potassium-transporting ATPase subunit α-3). ATP1A3 can bind to α-syn, thus impairing its activity [63]. Our results also confirmed the interaction between VAPB and CAMK2A (Calcium/calmodulin-dependent protein kinase type II subunit α). CAMK2A is a kinase that modulates calcium influx and synaptic function [64]. These results suggest that the interaction between p-α-syn and VAPB induce a synergistic role in calcium ions regulation and synaptic vesicle function.

In the current study, we exclusively examined the synergistic interaction p-α-syn and VAPB within the midbrain tissue of Tg mice under pathological conditions. Nonetheless, an expanding body of research suggests that phosphorylation at residue 129 site is also pertinent under physiological conditions [12, 45]. Notably, in our CO-IP experiments, we also detected an enrichment of p-α-syn using the p-α-syn antibody (CST, #23706; Supplementary material. Figure 1D-E) in the midbrain tissue of Wt mice. Based on these observations, we plan to employ the p-α-syn antibody as a tool to further investigate the distinct roles of p-α-syn in pathophysiological contexts.

Conclusions

Taken together, these findings indicate that p-α-syn antibody (CST, #23706) is a reliable tool for the detection and mechanistic studies of p-α-syn in PD and related pathologies. Besides, p-α-syn and VAPB can play a synergistic role in synaptic vesicle cycle and calcium reabsorption pathways under pathophysiologic situations. Importantly, this study supports the notion that phosphorylation at the serine 129 site of α-syn plays a crucial role in regulating its protein interactome, particularly in the interaction between α-syn and VAPB-PTPIP51, making it a potential target for the treatment of synucleinopathies.

Abbreviations

PD	Parkinson's Disease
α-syn	α-synuclein
h-α-syn	Human α-syn
m-α-syn	Mouse-α-syn
p-α-syn	pSer 129 α-syn, phosphorylation at the serine 129 site of α-syn
t-α-syn	Total α-syn

ER	Endoplasmic Reticulum
CO-IP/MS	Co-Immunoprecipitation and Mass Spectrometry
PPIs	Protein-Protein Interactions
MD	Molecular Dynamics
GO	Gene Ontology
KEGG	Kyoto Encyclopedia of Genes and Genomes
PTMs	Posttranslational Modifications
MAMs	Mitochondria-Associated Endoplasmic Reticulum Membranes
VAPB	The membrane tether Vesicle-Associated Membrane Protein Associated Protein B
PTPIP51	The outer mitochondrial membrane protein Tyrosine Phosphatase Interacting Protein 51
MSP	Major Sperm Protein
Tg	Transgenic
Wt	Wild-type
KO	Knock-Out
WB	Western Blotting
PVDF	Transferred to Polyvinylidene Difluoride
RT	Room Temperature
HRP	Horseradish Peroxidase
IP	Immunoprecipitation
CO-IP	Co-Immunoprecipitation
PFA	Paraformaldehyde
FBS	Fetal Bovine Serum
PME	Particle Mesh Ewald
IPTG	Isopropyl-β-D-1-Thiogalactopyranoside
PLK3	Polo-Like-Kinase 3
IAA	Iodoacetamide
FFAT	Two phenylalanines in an acidic tract
TM	Transmembrane domain
CC	Coiled-coil
TPR	Tetratricopeptide repeat
RMSD	Root Mean Square Deviation
RMSF	Root Mean Square Fluctuation
BP	Biological Processes
CCs	Cellular Components
MFs	Molecular Functions
CLTC	Clathrin Heavy Chain 1
ATP1A3	Sodium/potassium-transporting ATPase subunit α-3
CAMK2A	Calcium/Calmodulin-dependent Protein Kinase Type II Subunitα
TUBB4B	Tubulin β-4B chain
LBs	Lewy bodies

Supplementary Information

The online version contains supplementary material available at https://doi.org/10.1186/s40478-025-01949-6.

Supplementary Material 1: Table 7-Summary

Supplementary Material 2: Table 8-Tg-h-α-syn CO-IP-MS

Supplementary Material 3: Table 9-Tg-p-α-syn CO-IP-MS

Supplementary Material 4: Table 10-Wt-VAPB CO-IP-MS

Supplementary Material 5: Table 11-Tg-VAPB CO-IP-MS

Supplementary Material 6: Table 12 Statistical analysis of WB result

Supplementary Material 7: The full Blots Images

Supplementary Material 8: Figure 1

Supplementary Material 9: Figure 2

Supplementary Material 10: Figure 3

Supplementary Material 11: Figure 4

Supplementary Material 12: Figure 5

Supplementary Material 13: Figure legends of supplementary Figure 1-5

Acknowledgements
Not applicable.

Author contributions
W.J.L., Y.Y., and H.Y. conceived and designed the project. W.J.L., Y.Q.L., J.L. performed experiments and analyzed the data. W.J.L. prepared and wrote the manuscript. Y.Q.L., J.L., Y.Y., and H.Y. provided valuable comments and interpreted the results. Y.Y., and H.Y. supervised the whole study. All authors have reviewed and agreed to the published version of the manuscript.

Funding
This study was supported by the National Natural Science Foundation of China (No. 82301635), China Rehabilitation Science Institute's Fundamental Research Funds for the Central Public Welfare Research Institute (grant number: CRSI-82301635, 2023CZ-4) and the Chongqing Key Laboratory of Medical Emergency (NO.2022KFKT02).

Data availability
No datasets were generated or analysed during the current study.

Declarations

Ethics approval and consent to participate
Not applicable.

Consent for publication
All authors have read and agreed to the published version of the manuscript.

Competing interests
The authors declare no competing interests.

Author details
[1]China Rehabilitation Science Institute, Beijing, People's Republic of China
[2]China Rehabilitation Research Center, Feng tai District, Beijing, People's Republic of China
[3]Beijing Key Laboratory of Neural Injury and Rehabilitation, Feng tai District, Beijing, People's Republic of China
[4]School of Rehabilitation Medicine, Capital Medical University, Feng tai District, Beijing, People's Republic of China
[5]Center of Neural Injury and Repair, Beijing Institute for Brain Disorders, Feng tai District, Beijing, People's Republic of China
[6]Chongqing Key Laboratory of Emergency Medical, Chongqing Emergency Medical Center, Chongqing University Central Hospital, Chongqing, China
[7]Clinical Laboratory, Chongqing Emergency Medical Center, School of Medicine, Chongqing University Central Hospital, Chongqing University, Chongqing, China
[8]Beijing Institute of Brain Disorders, Laboratory of Brain Disorders, Hypoxia Conditioning Translational Laboratory of Clinical Medicine, Capital Medical University, Collaborative Innovation Center for Brain Disorders, Beijing Advanced Innovation Center for Big Data-based Precision Medicine, Capital Medical University, Beijing, China
[9]Department of Neurobiology, School of Basic Medical Sciences, Capital Medical University, Beijing 100069, China

Received: 26 November 2024 / Accepted: 5 February 2025
Published online: 24 February 2025

References

1. Park TY, Jeon J, Cha Y, Kim KS (2024) Past, present, and future of cell replacement therapy for parkinson's disease: a novel emphasis on host immune responses. Cell Res 34(7):479–492
2. Tanner CM, Ostrem JL (2024) Parkinson's Disease. N Engl J Med 391(5):442–452
3. Simuni T, Chahine LM, Poston K, Brumm M, Buracchio T, Campbell M et al (2024) A biological definition of neuronal alpha-synuclein disease: towards an integrated staging system for research. Lancet Neurol 23(2):178–190
4. Soto C (2024) Alpha-synuclein seed amplification technology for Parkinson's disease and related synucleinopathies. Trends Biotechnol 42(7):829–841

5. Surguchov A (2021) Invertebrate models untangle the mechanism of neurodegeneration in Parkinson's disease. Cells 10(2):407
6. Hassanzadeh K, Liu J, Maddila S, Mouradian MM (2024) Posttranslational modifications of alpha-Synuclein, their therapeutic potential, and Crosstalk in Health and neurodegenerative diseases. Pharmacol Rev 76(6):1254–1290
7. Anderson JP, Walker DE, Goldstein JM, de Laat R, Banducci K, Caccavello RJ et al (2006) Phosphorylation of Ser-129 is the dominant pathological modification of alpha-synuclein in familial and sporadic Lewy body disease. J Biol Chem 281(40):29739–29752
8. Zhou J, Broe M, Huang Y, Anderson JP, Gai WP, Milward EA et al (2011) Changes in the solubility and phosphorylation of alpha-synuclein over the course of Parkinson's disease. Acta Neuropathol 121(6):695–704
9. Samuel F, Flavin WP, Iqbal S, Pacelli C, Sri Renganathan SD, Trudeau LE et al (2016) Effects of Serine 129 phosphorylation on alpha-synuclein aggregation, Membrane Association, and internalization. J Biol Chem 291(9):4374–4385
10. Han R, Wang Q, Xiong X, Chen X, Tu Z, Li B et al (2024) Deficiency of Parkin causes neurodegeneration and accumulation of pathological alpha-synuclein in monkey models. J Clin Invest 134(20):e179633
11. Wang T, Liu W, Zhang Q, Jiao J, Wang Z, Gao G et al (2024) 4-Oxo-2-Nonenal- and agitation-Induced aggregates of alpha-synuclein and phosphorylated alpha-synuclein with distinct Biophysical properties and Biomedical Applications. Cells 13(9):739.
12. Parra-Rivas LA, Madhivanan K, Aulston BD, Wang L, Prakashchand DD, Boyer NP et al (2023) Serine-129 phosphorylation of alpha-synuclein is an activity-dependent trigger for physiologic protein-protein interactions and synaptic function. Neuron 111(24):4006–4023e10
13. Gibbons CH, Levine T, Adler C, Bellaire B, Wang N, Stohl J et al (2024) Skin biopsy detection of phosphorylated alpha-synuclein in patients with synucleinopathies. JAMA 331(15):1298–1306
14. McFarland MA, Ellis CE, Markey SP, Nussbaum RL (2008) Proteomics analysis identifies phosphorylation-dependent alpha-synuclein protein interactions. Mol Cell Proteom 7(11):2123–2137
15. Choi SG, Tittle T, Barot R, Betts D, Gallagher J, Kordower JH et al (2024) Comparing alpha-synuclein-interactomes between multiple systems atrophy and Parkinson's disease reveals unique and shared pathological features. bioRxiv[Preprint]. 21:2024.09.20.613717
16. Killinger BA, Marshall LL, Chatterjee D, Chu Y, Bras J, Guerreiro R et al (2022) In situ proximity labeling identifies Lewy pathology molecular interactions in the human brain. Proc Natl Acad Sci U S A 119(28):e2209742119.
17. Gomez-Suaga P, Bravo-San Pedro JM, Gonzalez-Polo RA, Fuentes JM, Niso-Santano M (2018) ER-mitochondria signaling in Parkinson's disease. Cell Death Dis 9(3):337
18. Larranaga-SanMiguel A, Bengoa-Vergniory N, Flores-Romero H (2024) Cross-talk between mitochondria-ER contact sites and the apoptotic machinery as a novel health meter. Trends Cell Biol35(1):33-45
19. Anderson AJ, Jackson TD, Stroud DA, Stojanovski D (2019) Mitochondria-hubs for regulating cellular biochemistry: emerging concepts and networks. Open Biol 9(8):190126
20. Coukos R, Krainc D (2024) Key genes and convergent pathogenic mechanisms in Parkinson disease. Nat Rev Neurosci 25(6):393–413
21. Subra M, Grimanelli Z, Gautier R, Mesmin B (2023) Stranger twins: a tale of resemblance and contrast between VAP proteins. Contact (Thousand Oaks) 6:25152564231183897
22. Kun-Rodrigues C, Ganos C, Guerreiro R, Schneider SA, Schulte C, Lesage S et al (2015) A systematic screening to identify de novo mutations causing sporadic early-onset Parkinson's disease. Hum Mol Genet 24(23):6711–6720
23. Paillusson S, Gomez-Suaga P, Stoica R, Little D, Gissen P, Devine MJ et al (2017) Alpha-synuclein binds to the ER-mitochondria tethering protein VAPB to disrupt ca(2+) homeostasis and mitochondrial ATP production. Acta Neuropathol 134(1):129–149
24. Guardia-Laguarta C, Area-Gomez E, Schon EA, Przedborski S (2015) A new role for alpha-synuclein in Parkinson's disease: alteration of ER-mitochondrial communication. Mov Disord 30(8):1026–1033
25. Yeo HK, Park TH, Kim HY, Jang H, Lee J, Hwang GS et al (2021) Phospholipid transfer function of PTPIP51 at mitochondria-associated ER membranes. EMBO Rep 22(6):e51323
26. Morotz GM, Martin-Guerrero SM, Markovinovic A, Paillusson S, Russell MRG, Machado PMP et al (2022) The PTPIP51 coiled-coil domain is important in VAPB binding, formation of ER-mitochondria contacts and IP3 receptor delivery of ca(2+) to mitochondria. Front Cell Dev Biol 10:920947
27. Guo M, Liu W, Luo H, Shao Q, Li Y, Gu Y et al (2023) Hypoxic stress accelerates the propagation of pathological alpha-synuclein and degeneration of dopaminergic neurons. CNS Neurosci Ther 29(2):544–558
28. Li R, Lu Y, Zhang Q, Liu W, Yang R, Jiao J et al (2022) Piperine promotes autophagy flux by P2RX4 activation in SNCA/alpha-synuclein-induced Parkinson disease model. Autophagy 18(3):559–575
29. Xiong HJ, Yu HQ, Zhang J, Fang L, Wu D, Lin XT et al (2023) Elevated FBXL6 activates both wild-type KRAS and mutant KRAS(G12D) and drives HCC tumorigenesis via the ERK/mTOR/PRELID2/ROS axis in mice. Mil Med Res 10(1):68
30. Jumper J, Evans R, Pritzel A, Green T, Figurnov M, Ronneberger O et al (2021) Highly accurate protein structure prediction with AlphaFold. Nature 596(7873):583–589
31. Abramson J, Adler J, Dunger J, Evans R, Green T, Pritzel A et al (2024) Accurate structure prediction of biomolecular interactions with AlphaFold 3. Nature 630(8016):493–500
32. Yan Y, Zhang D, Zhou P, Li B, Huang SY (2017) HDOCK: a web server for protein-protein and protein-DNA/RNA docking based on a hybrid strategy. Nucleic Acids Res 3;45 (W1): W365–W73
33. Liu W, Zhang Q, Xing H, Gao G, Liu J, Huang Y et al (2022) Characterization of a novel monoclonal antibody for Serine-129 phosphorylated alpha-Synuclein: a potential application for clinical and Basic Research. Front Neurol 13:821792
34. Wisniewski JR, Zougman A, Nagaraj N, Mann M (2009) Universal sample preparation method for proteome analysis. Nat Methods 6(5):359–362
35. Singleton AB, Farrer M, Johnson J, Singleton A, Hague S, Kachergus J et al (2003) Alpha-synuclein locus triplication causes Parkinson's disease. Science 302(5646):841
36. Eriksen JL, Przedborski S, Petrucelli L (2005) Gene dosage and pathogenesis of Parkinson's disease. Trends Mol Med 11(3):91–96
37. Polinski NK, Martinez TN, Ramboz S, Sasner M, Herberth M, Switzer R et al (2022) The GBA1 D409V mutation exacerbates synuclein pathology to differing extents in two alpha-synuclein models. Dis Model Mech 15(6):dmm049192
38. Gomez-Suaga P, Paillusson S, Stoica R, Noble W, Hanger DP, Miller CCJ (2017) The ER-Mitochondria Tethering Complex VAPB-PTPIP51 regulates Autophagy. Curr Biol 27(3):371–385
39. Obara CJ, Nixon-Abell J, Moore AS, Riccio F, Hoffman DP, Shtengel G et al (2024) Motion of VAPB molecules reveals ER-mitochondria contact site subdomains. Nature 626(7997):169–176
40. James C, Kehlenbach RH (2021) The interactome of the VAP family of proteins: an overview. Cells 10(7):1780
41. Di Mattia T, Martinet A, Ikhlef S, McEwen AG, Nomine Y, Wendling C et al (2020) FFAT motif phosphorylation controls formation and lipid transfer function of inter-organelle contacts. EMBO J 39(23):e104369
42. Zhang C, Pei Y, Zhang Z, Xu L, Liu X, Jiang L et al (2022) C-terminal truncation modulates alpha-synuclein's cytotoxicity and aggregation by promoting the interactions with membrane and chaperone. Commun Biol 5(1):798
43. Ramalingam N, Haass C, Dettmer U (2024) Physiological roles of alpha-synuclein serine-129 phosphorylation - not an oxymoron. Trends Neurosci 47(7):480–490
44. Sato H, Kato T, Arawaka S (2013) The role of Ser129 phosphorylation of alpha-synuclein in neurodegeneration of Parkinson's disease: a review of in vivo models. Rev Neurosci 24(2):115–123
45. Ramalingam N, Jin SX, Moors TE, Fonseca-Ornelas L, Shimanaka K, Lei S et al (2023) Dynamic physiological alpha-synuclein S129 phosphorylation is driven by neuronal activity. NPJ Parkinsons Dis 9(1):4
46. Rutherford NJ, Brooks M, Giasson BI (2016) Novel antibodies to phosphorylated alpha-synuclein serine 129 and NFL serine 473 demonstrate the close molecular homology of these epitopes. Acta Neuropathol Commun 4(1):80
47. Delic V, Chandra S, Abdelmotilib H, Maltbie T, Wang S, Kem D et al (2018) Sensitivity and specificity of phospho-Ser129 alpha-synuclein monoclonal antibodies. J Comp Neurol 526(12):1978–1990
48. Mori F, Nakamura Y, Miki Y, Tanji K, Kon T, Tomiyama M et al (2022) Alteration of Vesicle-Associated membrane protein-binding protein B in alpha-synuclein aggregates in Lewy Body Disease. J Neuropathol Exp Neurol 81(10):807–815
49. Mori F, Miki Y, Tanji K, Kon T, Tomiyama M, Kakita A et al (2021) Role of VAPB and vesicular profiles in alpha-synuclein aggregates in multiple system atrophy. Brain Pathol 31(6):e13001

50. Liu Y, Ma X, Fujioka H, Liu J, Chen S, Zhu X (2019) DJ-1 regulates the integrity and function of ER-mitochondria association through interaction with IP3R3-Grp75-VDAC1. Proc Natl Acad Sci U S A 116(50):25322–25328
51. Basso V, Marchesan E, Peggion C, Chakraborty J, von Stockum S, Giacomello M et al (2018) Regulation of ER-mitochondria contacts by Parkin via Mfn2. Pharmacol Res 138:43–56
52. Cali T, Ottolini D, Vicario M, Catoni C, Vallese F, Cieri D et al (2019) splitGFP technology reveals dose-dependent ER-mitochondria interface modulation by alpha-synuclein A53T and A30P mutants. Cells 8(9):1072
53. Huttlin EL, Ting L, Bruckner RJ, Gebreab F, Gygi MP, Szpyt J et al (2015) The BioPlex Network: a systematic exploration of the human interactome. Cell 162(2):425–440
54. Cali T, Ottolini D, Negro A, Brini M (2012) Alpha-synuclein controls mitochondrial calcium homeostasis by enhancing endoplasmic reticulum-mitochondria interactions. J Biol Chem 287(22):17914–17929
55. Dietel E, Brobeil A, Gattenlohner S, Wimmer M (2018) The importance of the right framework: mitogen-activated protein kinase pathway and the scaffolding protein PTPIP51. Int J Mol Sci 19(10):3282
56. Zhu X, Ruan Z, Yang X, Chu K, Wu H, Li Y et al (2015) Connexin 31.1 degradation requires the clathrin-mediated autophagy in NSCLC cell H1299. J Cell Mol Med 19(1):257–264
57. Wang X, Wei Z, Lan T, He Y, Cheng B, Li R et al (2022) CCDC88A/GIV promotes HBV replication and progeny secretion via enhancing endosomal trafficking and blocking autophagic degradation. Autophagy 18(2):357–374
58. Mahul-Mellier AL, Burtscher J, Maharjan N, Weerens L, Croisier M, Kuttler F et al (2020) The process of Lewy body formation, rather than simply alpha-synuclein fibrillization, is one of the major drivers of neurodegeneration. Proc Natl Acad Sci U S A 117(9):4971–4982
59. Fares MB, Jagannath S, Lashuel HA (2021) Reverse engineering Lewy bodies: how far have we come and how far can we go? Nat Rev Neurosci 22(2):111–131
60. Gomez-Suaga P, Perez-Nievas BG, Glennon EB, Lau DHW, Paillusson S, Morotz GM et al (2019) The VAPB-PTPIP51 endoplasmic reticulum-mitochondria tethering proteins are present in neuronal synapses and regulate synaptic activity. Acta Neuropathol Commun 7(1):35
61. Markovinovic A, Martin-Guerrero SM, Morotz GM, Salam S, Gomez-Suaga P, Paillusson S et al (2024) Stimulating VAPB-PTPIP51 ER-mitochondria tethering corrects FTD/ALS mutant TDP43 linked ca(2+) and synaptic defects. Acta Neuropathol Commun 12(1):32
62. Lindhout FW, Cao Y, Kevenaar JT, Bodzeta A, Stucchi R, Boumpoutsari MM et al (2019) VAP-SCRN1 interaction regulates dynamic endoplasmic reticulum remodeling and presynaptic function. EMBO J 38(20):e101345
63. Shrivastava AN, Triller A, Melki R (2020) Cell biology and dynamics of neuronal na(+)/K(+)-ATPase in health and diseases. Neuropharmacology 169:107461
64. Hell JW (2023) Binding of CaMKII to the NMDA receptor is sufficient for long-term potentiation. Sci Signal 16(808):eadk9224

Publisher's note